Journal of Vibration Engineering & Technologies (2024) 12:1225–1247
https://doi.org/10.1007/s42417-023-00903-x

ORIGINAL PAPER

Dynamic Analysis of Coupled Axial-Bending Wave Propagation in a Cracked Timoshenko Beam Using Spectral Finite-Element Method

Krishna Modak[1] · T. Jothi Saravanan[1] · Shanthanu Rajasekharan[2]

Received: 15 November 2022 / Revised: 1 February 2023 / Accepted: 10 February 2023 / Published online: 11 March 2023

Abstract

Purpose The coupling between axial, transverse shear, and bending deformations is significant for beam-like lattice structures in structural mechanics where beam theory is applied. Likewise, periodic large lattice structures like frames and trusses experience extension-transverse shear-bending coupled vibrations, which the coupled axial-bending Timoshenko beam theory can describe well.

Methods This paper introduces a general approach using the spectral finite-element method for a single edge notch cracked Timoshenko beam for wave propagation analysis and damage detection. Besides, the present work has developed a spectral element model for the classical coupled axial-bending Timoshenko beam theory and cracked beam theory along with the spectral throw-off elements. The crack introduced is a transverse open and non-propagating crack. The cracked region is discretized into a massless and dimensionless spring element for spectral analysis. The quantity of damage implemented is expressed in crack flexibility based on fracture mechanics, and the compatibility conditions are satisfied at the damage region. The variation in wave propagation analysis is studied in the presence of crack by comparing responses from damaged and undamaged coupled axial-bending Timoshenko beams without coupling coefficients.

Results The crack depth and location effects are examined through numerical investigations of the various wave propagation phenomena. The responses collected from different points are presented, and the proper analysis of these responses accurately indicates the damage location. Correspondingly, the investigation for modal analysis is also carried out on the proposed coupled axial-bending Timoshenko beam model with coupling coefficients. The free-vibration analyses for beam models with and without crack conditions are investigated for clamped-free and simply–simply supported boundary conditions. The estimated modal frequencies and mode shapes agree with the existing methods. Thus, the proposed spectral element for the coupled axial-bending cracked Timoshenko beam model is promising for future work with damaged structures with more complex geometry.

Keywords Spectral finite-element method · Cracked Timoshenko beam · Wave propagation · Non-propagating crack · Damage detection · Coupling

Introduction

Over the past few decades, there has been an interest in infrastructure monitoring and damage detection. It emphasizes incorporating technological developments to make it more advanced [1]. The dynamic behavior of structures generally follows the laws of non-linearity, which are often associated with geometry and boundary conditions [2]. The degree of damage can be determined by the decrease in dynamic stiffness and the increase in damping. It does not matter whether this damage is localized like a crack or distributed in most samples by the number of micro-cracks. Local or distributed stiffness changes can lead to changes in the natural frequency of the structure [3, 4]. The traditional modal analysis method is often appropriate for structures, which can be modeled by discrete elements of grouped parameters, where the presence of damage leads to a low-frequency change in the system's overall behavior. On the other side, small defects, such as cracks, are hidden by modal approaches,

✉ T. Jothi Saravanan
tjs@iitbbs.ac.in

[1] School of Infrastructure, Indian Institute of Technology Bhubaneswar, Kansapada, Odisha 752-050, India

[2] ASTER Co., Ltd, Tokyo 104-0028, Japan

since such phenomena are high-frequency effects that cannot easily be discovered by examining changes in modal mass, stiffness, or damping parameters [5, 6].

Many analytical methods have been developed to solve wave propagation problems. This includes Fourier synthesis, popularly known as the spectral finite-element method (SFEM) [7–12].

F. Pind et al. [13] have developed a method for simulating room acoustics in the time domain using a combination of a spectral element method and an implicit–explicit Runge–Kutta time stepping method. This method has low dispersion and dissipation, can handle adaptive, unstructured meshes with curvilinear elements, and is suitable for parallel implementation. Wu Z et al. [14] present a new type of lattice structure with a two-order hierarchical periodicity, inspired by the structure of butterfly wings, has been designed and the band-gap properties have been investigated using the spectral element method. The dynamic behavior of the structure has been analyzed, and it was found to have distinct macro- and micro-stop-bands in the given frequency domain. The mechanisms for these band-gaps and the relationship between the hierarchical periodicities and the stop-bands were also explored. The efficiency of the spectral element method was validated by comparing the results with those obtained using the finite-element method. ZJ Wu et al. [15] study the dynamic properties of three-dimensional piezoelectric Kagome grids were analyzed to understand their ability to transform mechanical energy into electric energy and their performance in vibration isolation. The spectral element method (SEM) was used to solve the equation of motion for the structure and accurately determine the frequency-domain responses. The results were compared with those obtained using the finite-element method (FEM) and with those from previous literature, and it was found that the SEM was effective in studying 3D piezoelectric Kagome grids. ZJ Wu [16] also studied about the vibration characteristics of sandwich panels with corrugated cores were analyzed using the spectral element method (SEM). The SEM was used to establish spectral equations for plate elements with both in-plane and out-of-plane components, and the spectral stiffness matrix for the entire structure was assembled. The frequency responses were then obtained by calculating the spectral equations. The results showed that the SEM was effective in studying the vibration band-gap properties of sandwich panels with corrugated cores, and that it was able to produce more accurate results than the finite-element method (FEM). WJ Wu [17] presents a study to investigate the vibration band-gap properties of three-dimensional (3D) Kagome lattices. The SEM was able to accurately and effectively analyze the vibration characteristics of the 3D Kagome lattices by deriving the dynamic stiffness matrix of the 3D element and establishing the spectral equations of motion for the entire lattice structure. The results were compared with those obtained using the finite-element method (FEM) and it was found that the SEM was suitable for analyzing the vibration band-gap properties of 3D Kagome lattices. A Mukherjee et al. [18] propose numerical method to solve the nonlinear eigenvalue problem (NLEP) in SEM. NLEP cannot be solved using linear numerical eigen-solvers, so two distinct numerical methods were proposed to compute the eigenvalues of the problem more efficiently using SEM. These methods were a root finding method of rational polynomial functions and a linearization of Lagrange matrix interpolating polynomials. The proposed methods were able to solve NLEP in a stable, efficient, and accurate way, even in the presence of singularities. The accuracy of the methods was numerically evaluated by comparing the solutions obtained with those from modal analysis using the finite-element method (FEM). Loya et al. [19] present a view on methods for detecting cracks and knowing about their nature by finding natural frequencies for bending vibrations of the cracked beam. The beam is modeled as two segments connected by an extensional and rotational spring. The results from the perturbative method agree with those obtained with the direct method. A study is proposed to examine the vibrational properties of axially loaded Euler–Bernoulli and Timoshenko beams with arbitrary cracks. The cracks in beams are modeled as transversely open and non-propagating. A massless rotational spring models the cracking on a beam under axial loading [20, 21]. A new crack localization algorithm based on a mathematical model is proposed, which describes the lateral vibration of a rotating cracked Timoshenko beam. This model is derived using Lagrange equations and the assumed mode method [22]. Shi et al. [23] present an accurate solution method for the free vibrations of Timoshenko beams with general elastic restraints at the endpoints. Generally, the method is applied to a wide range of boundary conditions without modifying solution algorithms and procedures.

Efficient vibration analysis of one-dimensional (1D) lattice (or periodic) structures, the so-called spectral transfer matrix method (STMM), is introduced by combining the good features of SFEM with a well-known transfer matrix method. The efficiency of the proposed method is proven in the solution of Bernoulli–Euler beams and large planar lattice structures [24]. Unlike traditional finite elements, the length of spectral elements is not a limiting factor. Each element is formulated exactly, regardless of its length. Therefore, structural connection and discontinuities control the length of the element [25]. A new matrix formulation is presented to analyze the dynamic response and propagation of elastic waves in the structure consisting of beams and rods connected by rigid or pinned joints. Their methods showed higher accuracy than the existing FEM in evaluating the natural frequencies of framed structures [26].

A new plate element is developed using SFEM with cracks along its length. The elastic behavior of the plate at the crack position is considered a line spring with various stiffnesses along the crack length [27, 28]. An approach is developed for the flow characteristics of the vibrational force of open cracks in the Timoshenko beam structure. The results indicate that the flow characteristics are unusually related to the crack position and depth, especially at high frequencies [29]. Kudela et al. [30] present a new spectral finite element of the composite plate. The wave propagation analysis using transverse elastic waves is carried out on the element for various orientations and relative volume fractions of reinforcing fibers. The modeling of wave propagation in plate structure using 3D-SFEM is studied for damage identification [31]. The Love rod theory proposes the formulation for coupled axial–flexural wave interaction in a sagged rod using SFEM [32]. Structural damage detection through axial–flexural wave interaction using SFEM is established for rod and beam structure [33]. The experimental investigation using piezoelectric transducers is proposed under narrowband amplitude-modulated excitation force for coupled axial–flexural wave propagation in a sagged rod with structural discontinuity [34]. The dynamic stiffness matrix of the Timoshenko beam under moving load with constant velocity and acceleration subjected to an open crack is derived using SFEM. The modeling is done by two rotational and extensional massless springs [35].

Numerous civil/mechanical structures are demonstrated as beams for the dynamic analysis, employing classical Euler–Bernoulli or Timoshenko beam theories. However, several structural members have coupling interactions from various fundamental deformation modes, which conventional beam theories do not deal with reasonably [36, 37]. Recently, the stiffness theory was established by developing the governing differential equations of motion of the coupled axial-bending beam using Hamilton's principle [38, 39]. Still, substantial literature is unavailable for the dynamic analysis of the coupled axial-bending wave propagation problem in SFEM. This paper has developed a spectral element model for the coupled axial-bending Timoshenko beam element. Equally, the main focus is to understand the cracked Timoshenko beam element. From the previous literature, it can be understood that the Timoshenko beam theory makes an excellent candidate to combine with crack mechanics, making it a general theory for any spectral analysis.

Firstly, this article attempts to unify the theory of the SFEM for the Timoshenko beam and fracture mechanics in the frequency domain, making it simpler for wave propagation and modal analysis with coupled axial-bending effects. An open non-propagating transverse-single edge crack opening is investigated in the present work. Furthermore, the variation in wave propagation analysis is studied in the presence of crack by comparing responses from damaged and undamaged coupled axial-bending Timoshenko beams without coupling coefficients. Then, the effect of crack depth and location is studied for the various wave propagation phenomena. Correspondingly, the modal analyses are carried out to investigate the crack formation effect with the coupling coefficients using STMM. Finally, the parametric study is carried out to understand the variation of coupling coefficients for crack formation. The proposed spectral element for the coupled axial-bending cracked Timoshenko beam model has been shown to analyze the damaged structures and precisely identify and evaluate the crack location.

Equation of Motion for a Coupled Axial-Bending Timoshenko Beam

The following equation expresses the planar motion of a coupled axial-bending Timoshenko beam as:

$$\begin{bmatrix} N_t' \\ Q_t' \\ M_t' \end{bmatrix} = \begin{bmatrix} \rho A & 0 & \rho R \\ 0 & \rho A & 0 \\ \rho R & 0 & \rho I \end{bmatrix} \begin{bmatrix} \ddot{u} \\ \ddot{w} \\ \ddot{\theta} \end{bmatrix} - \begin{bmatrix} 0 \\ 0 \\ Q_t \end{bmatrix}. \tag{1}$$

Here, $N_t(x, y)$, $Q_t(x, y)$, and $M_t(x, y)$ are axial tensile forces, lateral shear forces, and bending moments, respectively, where the prime (') represents the derivative with respect to the spatial coordinate along the longitudinal axis of the beam, say x; $u(x, y)$, $w(x, y)$, and $\theta(x, y)$ are axial and lateral displacement and rotation, respectively; ρA, ρR, and ρI are the effective mass per length, the first-order moment of inertia, and the second-order moment of inertia. It is expressed as

$$\rho A = \int \rho dA, \rho R = \int \rho z dA, \rho I = \int \rho z^2 dA, \tag{2}$$

where ρ is the mass density per unit volume and A is the cross-section area. The force–displacement relationship for a coupled axial-bending Timoshenko beam is represented by

$$\begin{bmatrix} N_t \\ Q_t \\ M_t \end{bmatrix} = \begin{bmatrix} EA & C_1 & C_2 \\ C_1 & GA & C_3 \\ C_2 & C_3 & EI \end{bmatrix} \begin{bmatrix} u' \\ w' - \theta \\ \theta' \end{bmatrix} - \begin{bmatrix} 0 \\ 0 \\ Q_t \end{bmatrix}, \tag{3}$$

where EA, GA, and EI are axial, shear, and flexural rigidity, respectively; C_1, C_2, and C_3 are the coupling stiffnesses representing the interaction between axial, lateral shear, and bending deformations. The decoupled equations of motion of the classical Timoshenko beam and longitudinal rod are obtained when all ρR, C_1, C_2, and C_3 parameters are ignored [40]. The coupled axial-bending Timoshenko beam theory represented by Eq. (1) is applied to a homogenized beam model of a 1D periodic lattice structure whose cross-section

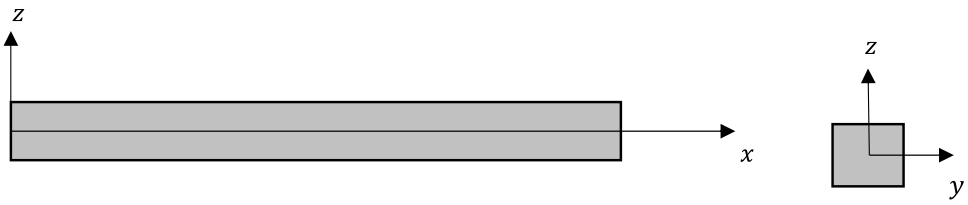

Fig. 1 The coordinate system for a coupled axial-bending Timoshenko beam

is symmetric with respect to the vertical axis (z -axis). The beam model takes the extension-transverse shear-bending coupled in-plane vibration in the $x-z$ plane without torsion about the elastic axis (x -axis), as shown in Fig. 1.

Mathematical Framework: Spectral Finite-Element Method

According to SFEM, analyzing frequencies with one spectral element in any range is possible. It is important to analyze high natural frequencies, as slight imperfections could cause noticeable changes. In such cases, the classical FEM involves a very dense grid and is time-consuming to calculate. For the classical FEM models, elements of the dynamic stiffness matrix in the frequency domain are nearly constant for higher frequencies, and there is an additional mathematical computation needed. The spectral approach provides a dynamically changing stiffness matrix in a whole frequency range. There are three specific cases for wave propagation in the connected waveguide. The first is that members are connected at both ends, called a double-nodded element. It conducts energy in both directions. The second is when members connect at one point and expand to infinity by conducting energy in one direction without reflection, called a single-nodded or a throw-off element. These elements act as an infinite medium to transfer energy out of the system. Both behaviors are fundamentally different and need to be handled separately. The third is the presence of local discontinuity along the length of the structure. It is complex to model waveguide elements with local discontinuity, such as holes, cracks, or joints.

Finite Spectral Element Formulation

The spectral displacement field is expressed to construct the spectral elements of a coupled axial-bending Timoshenko beam, based on the discrete Fourier transform theory, as follows:

$$\begin{aligned} u(x,t) &= \sum_{n=0}^{N-1} \overline{u}_n(x) e^{i\omega_n t} \\ w(x,t) &= \sum_{n=0}^{N-1} \overline{w}_n(x) e^{i\omega_n t} \\ \theta(x,t) &= \sum_{n=0}^{N-1} \overline{\theta}_n(x) e^{i\omega_n t}, \end{aligned} \tag{4}$$

where $\overline{u}_n$, $\overline{w}_n$, and $\overline{\theta}_n$ ($n=0, 1, 2, \ldots, N\text{-}1$) are the Fourier component of $u(x,y)$, $w(x,y)$, and $\theta(x,y)$, respectively. Each corresponds to the discrete frequency defined by $\omega_n = 2\pi n/T_t$, where T_t is the time window (period). It is related to the number of samples as $N = 2f_{NQY}T_t$; where f_{NQY} is the Nyquist frequency. Similarly, the axial tensile force $T(x,y)$, lateral shear force $Q(x,y)$, and bending moment $M(x,y)$ are expressed in a spectral format as follows:

$$\begin{aligned} T(x,t) &= \sum_{(n=0)}^{N-1} \overline{T}_n(x) e^{(i\omega_n t)} \\ Q(x,t) &= \sum_{n=0}^{N-1} \overline{Q}_n(x) e^{i\omega_n t} \\ M(x,t) &= \sum_{n=0}^{N-1} \overline{M}_n(x) e^{i\omega_n t}. \end{aligned} \tag{5}$$

The subscript n for the nth Fourier component is omitted in the following derivations to simplify the process. Substitution of Eqs. (4) and (5) into Eqs. (1) and (3) gives

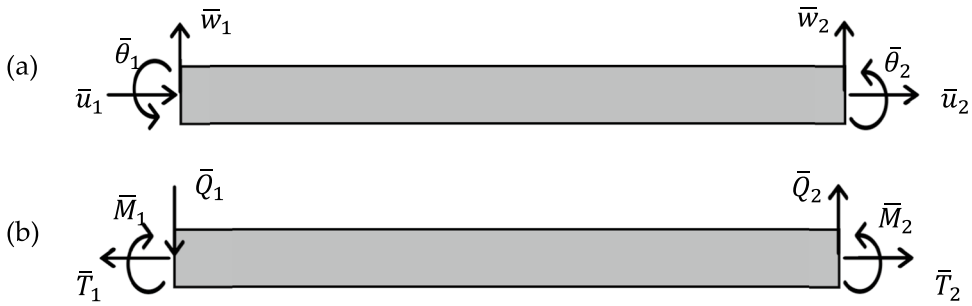

Fig. 2 Sign conventions assumed for **a** nodal displacements and **b** nodal forces for finite spectral element formulation

$$\begin{bmatrix} \overline{T}' \\ \overline{Q}' \\ \overline{M}' \end{bmatrix} = -\omega^2 \begin{bmatrix} \rho A & 0 & \rho R \\ 0 & \rho A & 0 \\ \rho R & 0 & \rho I \end{bmatrix} \begin{bmatrix} \ddot{u} \\ \ddot{w} \\ \ddot{\theta} \end{bmatrix} - \begin{bmatrix} 0 \\ 0 \\ Q_t \end{bmatrix} \tag{6}$$

and

$$\begin{bmatrix} \overline{T} \\ \overline{Q} \\ \overline{M} \end{bmatrix} = \begin{bmatrix} EA & C_1 & C_2 \\ C_1 & GA & C_3 \\ C_2 & C_3 & EI \end{bmatrix} \begin{bmatrix} \overline{u}' \\ \overline{w}' - \overline{\theta} \\ \overline{\theta}' \end{bmatrix}. \tag{7}$$

By substituting Eq. (6) into Eq. (7), the governing equations are derived as

$$\begin{bmatrix} EA & C_1 & C_2 \\ C_1 & GA & C_3 \\ C_2 & C_3 & EI \end{bmatrix} \begin{bmatrix} \overline{u}'' \\ \overline{w}'' \\ \overline{\theta}'' \end{bmatrix} + \begin{bmatrix} 0 & 0 & -C_1 \\ 0 & 0 & -GA \\ C_1 & GA & 0 \end{bmatrix} \begin{bmatrix} \overline{u}' \\ \overline{w}' \\ \overline{\theta}' \end{bmatrix} - \begin{bmatrix} 0 & 0 & 0 \\ 0 & 0 & 0 \\ 0 & 0 & GA \end{bmatrix} \begin{bmatrix} \overline{u} \\ \overline{w} \\ \overline{\theta} \end{bmatrix} + \omega^2 \begin{bmatrix} \rho A & 0 & \rho R \\ 0 & \rho A & 0 \\ \rho R & 0 & \rho I \end{bmatrix} \begin{bmatrix} \overline{u} \\ \overline{w} \\ \overline{\theta} \end{bmatrix} = \begin{bmatrix} 0 \\ 0 \\ 0 \end{bmatrix}. \tag{8}$$

Assuming the general solution of Eq. (8) as

$$\overline{u}(x) = \alpha W e^{-ikx}, \overline{w}(x) = W e^{-ikx}, \overline{\theta}(x) = \beta W e^{-ikx}, \tag{9}$$

where k is the wavenumber. Substitution of Eq. (9) into Eq. (8) gives

$$X(k) W \begin{bmatrix} \alpha \\ 1 \\ \beta \end{bmatrix} = \begin{bmatrix} 0 \\ 0 \\ 0 \end{bmatrix}, \tag{10}$$

where

$$X(k) = \begin{bmatrix} -k^2 EA + \omega^2 \rho A & -k^2 C_1 & ikC_1 - k^2 C_2 + \omega^2 \rho R \\ -k^2 C_1 & -k^2 GA + \omega^2 \rho A & ikGA - k^2 C_3 \\ -ikC_1 - k^2 C_2 + \omega^2 \rho R & -ikGA - k^2 C_3 & -k^2 EI + \omega^2 \rho I - GA \end{bmatrix}. \tag{11}$$

From Eq. (11), the dispersion equation is written as

$$X(k) = a_1 k^6 + a_2 k^4 + a_3 k^2 + a_4 = 0, \tag{12}$$

where

$$a_1 = EIC_1^2 - 2C_1 C_2 C_3 + GAC_2^2 + EAC_3^2 - EAEIGA$$

$$a_2 = 2C_1 C_3 \rho R \omega^2 - C_3^2 \rho A \omega^2 - C_1^2 \rho I \omega^2 - 2C_2 GA \rho R \omega^2 + EAEI \rho A \omega^2 + EAGA \rho I \omega^2 + EIGA \rho A \omega^2$$

$$a_3 = GA \rho \mathrm{R}^2 \omega^2 - EI \rho A^2 \omega^4 - C_1^2 \rho A \omega^2 + EAGA \rho A \rho R \omega^4 - EA \rho A \rho I \omega^4 + EIGA \rho A \omega^2$$

$$a_4 = \rho I \rho A^2 \omega^6 - GA \rho A^2 \omega^4 - \rho A \rho R^2 \omega^6.$$

The six roots of Eq. (12) are obtained as follows:

$$\begin{aligned} &k_1 = -k_4 \quad k_2 = -k_5 \quad k_3 = -k_6 \\ &k_1 = \left(-\frac{1}{3} b_2 - \frac{1}{2}(B + C) - i \frac{\sqrt{3}}{2}(B - C) \right)^{\frac{1}{2}} \\ &k_2 = \left(-\frac{1}{3} b_2 - \frac{1}{2}(B + C) - i \frac{\sqrt{3}}{2}(B - C) \right)^{\frac{1}{2}} \\ &k_3 = \left(-\frac{1}{3} b_2 + (B + C) \right)^{\frac{1}{2}}, \end{aligned} \tag{13}$$

where

$$\begin{aligned} &B = \left(P + \sqrt{D} \right)^{\frac{1}{3}}, \quad C = \left(P - \sqrt{D} \right)^{\frac{1}{3}}, \quad D = O^3 + P^2 \\ &O = \frac{3b_1 - b_2^2}{9}, \quad P = \frac{9b_2 b_1 - 27b_0 - 2b_2^3}{54} \\ &b_0 = \frac{a_4}{a_1}, \quad b_1 = \frac{a_3}{a_1}, \quad b_2 = \frac{a_2}{a_1}. \end{aligned} \tag{14}$$

From Eq. (10), α_n and β_n are determined as

$$\begin{aligned} c\alpha_n &= \left(\rho A \rho R \omega^4 - C_1 C_3 k^4 + C_2 GAk^4 - C_2 k^2 \rho A \omega^2 - GAk^2 \rho R \omega^2 + iC_1 k \rho A \omega^2 \right) / \Delta \beta_n \\ &= \left(C_1^2 k^4 - \rho A^2 \omega^4 - EAGAk^4 + EAk^2 \rho A \omega^2 + GAk^2 \rho A \omega^2 \right) / \Delta \Delta \\ &= \left(k \left(iC_1^2 k^2 - C_2 C_1 k^3 + \rho R C_1 k \omega^2 + C_3 EAk^3 - iEAGAk^2 - C_3 \rho A k \omega^2 + iGA \rho A \omega^2 \right) \right). \end{aligned} \tag{15}$$

Using the six wavenumbers computed in Eq. (13), the general solution for an element is expressed in the form of

$$\begin{aligned}
c\overline{u}(x) &= \alpha_1 W_1 e^{-ik_1 x} + \alpha_2 W_2 e^{-ik_2 x} + \alpha_3 W_3 e^{-ik_3 x} \\
&\quad + \alpha_4 W_4 e^{-ik_1 (L-x)} + \alpha_5 W_5 e^{-ik_2 (L-x)} + \alpha_6 W_6 e^{-ik_3 (L-x)} \\
\overline{w}(x) &= W_1 e^{-ik_1 x} + W_2 e^{-ik_2 x} + W_3 e^{-ik_3 x} \\
&\quad + W_4 e^{-ik_1 (L-x)} + W_5 e^{-ik_2 (L-x)} + W_6 e^{-ik_3 (L-x)} \\
\overline{\theta}(x) &= \beta_1 W_1 e^{-ik_1 x} + \beta_2 W_2 e^{-ik_2 x} + \beta_3 W_3 e^{-ik_3 x} \\
&\quad + \beta_4 W_4 e^{-ik_1 (L-x)} + \beta_5 W_5 e^{-ik_2 (L-x)} + \beta_6 W_6 e^{-ik_3 (L-x)}.
\end{aligned} \tag{16}$$

Figure 2 illustrates the sign conventions assumed for nodal displacements and nodal forces for finite spectral element formulation. Substituting the boundary conditions of nodal displacements gives

$$\begin{bmatrix} \overline{u}_1 \\ \overline{w}_1 \\ \overline{\theta}_1 \\ \overline{u}_2 \\ \overline{w}_2 \\ \overline{\theta}_2 \end{bmatrix} = \begin{bmatrix} \overline{u}(0) \\ \overline{w}(0) \\ \overline{\theta}(0) \\ \overline{u}(L) \\ \overline{w}(L) \\ \overline{\theta}(L) \end{bmatrix} = [\boldsymbol{T}_1] \begin{bmatrix} W_1 \\ W_2 \\ W_3 \\ W_4 \\ W_5 \\ W_6 \end{bmatrix}. \tag{17}$$

By substituting Eq. (16) into Eq. (7), the balancing nodal forces for an element gives

$$\begin{bmatrix} \overline{T}_1 \\ \overline{Q}_1 \\ \overline{M}_1 \\ \overline{T}_2 \\ \overline{Q}_2 \\ \overline{M}_2 \end{bmatrix} = \begin{bmatrix} -\overline{T}(0) \\ -\overline{Q}(0) \\ -\overline{M}(0) \\ \overline{T}(L) \\ \overline{Q}(L) \\ \overline{M}(L) \end{bmatrix} = [\boldsymbol{T}_2] \begin{bmatrix} W_1 \\ W_2 \\ W_3 \\ W_4 \\ W_5 \\ W_6 \end{bmatrix}. \tag{18}$$

Combining Eq. (18) and Eq. (17) gives

$$\begin{bmatrix} \overline{T}_1 \\ \overline{Q}_1 \\ \overline{M}_1 \\ \overline{T}_2 \\ \overline{Q}_2 \\ \overline{M}_2 \end{bmatrix} = [\boldsymbol{T}_2][\boldsymbol{T}_1]^{-1} \begin{bmatrix} \overline{u}_1 \\ \overline{w}_1 \\ \overline{\theta}_1 \\ \overline{u}_2 \\ \overline{w}_2 \\ \overline{\theta}_2 \end{bmatrix}. \tag{19}$$

From Eq. (19), the frequency-dependent dynamic stiffness matrix for a finite spectral element is expressed as

$$S(\omega) = [\boldsymbol{T}_2][\boldsymbol{T}_1]^{-1}. \tag{20}$$

$[\boldsymbol{T}_1]$ *and* $[\boldsymbol{T}_2]$ are presented in the Appendix section; refer to Equation (A2) and Equation (A3), respectively.

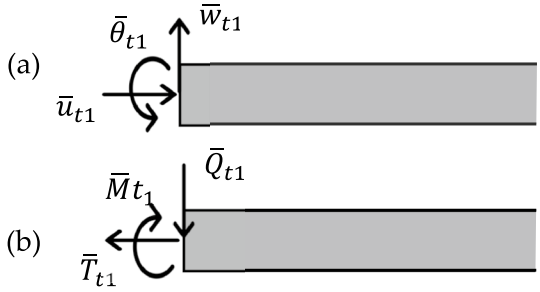

Fig. 3 Sign conventions defined for **a** nodal displacements and **b** nodal forces for throw-off spectral element formulation

Throw-off Spectral Element Formulation

A throw-off element is developed to capture only either forward or backward propagating waves. Figure 3 represents the nodal displacements and nodal forces for the throw-off spectral element. Similarly, the frequency-dependent dynamic stiffness matrix can be derived for the throw-off spectral element.

From Eq. (16), the general solution reduces to: (as $L = \infty$)

$$\begin{aligned}
\overline{u}_t(x) &= \alpha_1 W_1 e^{-ik_1 x} + \alpha_2 W_2 e^{-ik_2 x} + \alpha_3 W_3 e^{-ik_3 x} \\
\overline{w}_t(x) &= W_1 e^{-ik_1 x} + W_2 e^{-ik_2 x} + W_3 e^{-ik_3 x} \\
\overline{\theta}_t(x) &= \beta_1 W_1 e^{-ik_1 x} + \beta_2 W_2 e^{-ik_2 x} + \beta_3 W_3 e^{-ik_3 x}.
\end{aligned} \tag{21}$$

Substituting nodal displacement shown in Fig. 3 gives

$$\begin{bmatrix} \overline{u}_{t1} \\ \overline{w}_{t1} \\ \overline{\theta}_{t1} \end{bmatrix} = \begin{bmatrix} \overline{u}_t(0) \\ \overline{w}_t(0) \\ \overline{\theta}_t(0) \end{bmatrix} = [\boldsymbol{T}_{t1}] \begin{bmatrix} W_1 \\ W_2 \\ W_3 \end{bmatrix}. \tag{22}$$

By substituting Eq. (22) in Eq. (8), the balancing nodal forces are expressed as

$$\begin{bmatrix} \overline{T}_{t1} \\ \overline{Q}_{t1} \\ \overline{M}_{t1} \end{bmatrix} = \begin{bmatrix} -\overline{T}_t(0) \\ -\overline{Q}_t(0) \\ -\overline{M}_t(0) \end{bmatrix} = [\boldsymbol{T}_{t2}] \begin{bmatrix} W_1 \\ W_2 \\ W_3 \end{bmatrix}. \tag{23}$$

Combining Eq. (23) and Eq. (22) gives

$$\begin{bmatrix} \overline{T}_t \\ \overline{Q}_t \\ \overline{M}_t \end{bmatrix} = [\boldsymbol{T}_{t2}][\boldsymbol{T}_{t1}]^{-1} \begin{bmatrix} \overline{u}_t \\ \overline{w}_t \\ \overline{\theta}_t \end{bmatrix}. \tag{24}$$

Om Eq. (24), the frequency-dependent dynamic stiffness matrix for a throw-off spectral element is expressed as

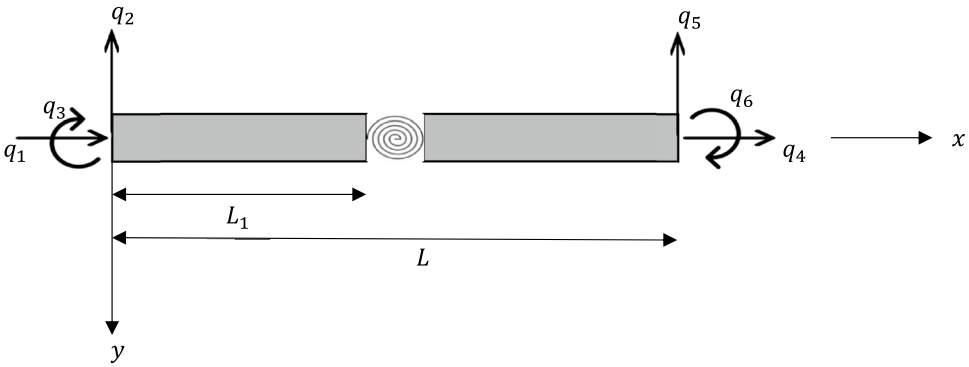

Fig. 4 A coupled axial-bending Timoshenko beam model with a transverse open and non-propagating crack simulated by an elastic hinge

$$S_{t(\omega)} = \left[T_{t2}\right]\left[T_{t1}\right]^{-1}. \tag{25}$$

$\left[T_{t1}\right] and \left[T_{t2}\right]$ are explained in the Appendix section; refer to Equation (A5) and Equation (A6), respectively. The spectral elements in Eqs. (20) and (25) can be analogously assembled in the conventional FEM. After applying the relevant boundary conditions, a global dynamic stiffness matrix equation can be obtained.

Coupled Axial-Bending Cracked Timoshenko Beam Formulation

Figure 4 shows a finite spectral element of a coupled axial-bending Timoshenko beam with an open transverse and non-propagating crack. The length of the element is L, and its cross-sectional area is A. The crack is replaced by a dimensionless-massless spring, the flexibility of which is calculated using the Castigliano Theorem and laws of fracture mechanics [41, 42]. The spectral nodal displacements $\overline{u}$ and $\overline{w}$, and rotations $\overline{\theta}$ are presumed for the left and right parts of the beam as follows:

where L_1 is the location of the crack from the left, and the amplitude ratios α_n and β_n are determined from Eq. (15), respectively.

The coefficients in Eq. (26), $A_1, B_1, \in_1, D_1, E_1 F_1, A_2, B_2, \in_2, D_2, E_2, F_2$ are calculated from the following boundary conditions:

- At the left end of the element ($x = 0$)

$$\begin{aligned} u_1(x) &= q_1 \\ u_1(x) &= q_1 \\ w_1(x) &= q_2 \\ \theta_1(x) &= q_3. \end{aligned} \tag{27}$$

- At the right end of the element ($x = L$)

$$\begin{aligned} u_2(x) &= q_4 \\ w_2(x) &= q_5 \\ \theta_2(x) &= q_6. \end{aligned} \tag{28}$$

- At crack location (a total change of displacements and rotation angle, compatibility of bending

$$\begin{aligned} \overline{u_1} &= A_1\alpha_1 e^{(-ik_1x)} + B_1\alpha_2 e^{(-ik_2x)} + \in_1 \alpha_3 e^{(-ik_3x)} + D_1\alpha_4 e^{(-ik_1(L_1-x))} + E_1\alpha_5 e^{(-ik_2(L_1-x))} + F_1\alpha_6 e^{(-ik_3(L1-x))} for x \in (0, L_1) \\ \overline{w_1} &= A_1 e^{(-ik_1x)} + B_1 e^{(-ik_2x)} + \in_1 e^{(-ik_3x)} + D_1 e^{(-ik_1(L_1-x))} + E_1 e^{(-ik_2(L_1-x))} + F_1 e^{(-ik_3(L_1-x))} for x \in (0, L_1) \\ \overline{\theta_1} &= A_1\beta_1 e^{(-ik_1x)} + B_1\beta_2 e^{(-ik_2x)} + \in_1 \beta_3 e^{(-ik_3x)} + D_1\beta_4 e^{(-ik_1(L_1-x))} + E_1\beta_5 e^{(-ik_2(L_1-x))} + F_1\beta_6 e^{(-ik_3(L_1-x))} for x \in (0, L_1) \\ \overline{u_2} &= A_2\alpha_1 e^{(-ik_1(L_1+x))} + B_2\alpha_2 e^{(-ik_2(L_1+x))} + \in_2 \alpha_3 e^{(-ik_3(L_1+x))} + D_2\alpha_4 e^{(ik_1(L_1-L+x))} + E_2\alpha_5 e^{(ik_2(L_1-L+x))} \\ &\quad + F_2\alpha_6 e^{(ik_3(L_1-L+x))} for x \in (0, L-L_1) \overline{w_2} = A_2 e^{(-ik_1(L_1+x))} + B_2 e^{(-ik_2(L_1+x))} + \in_2 e^{(-ik_3(L_1+x))} \\ &\quad + D_2 e^{(ik_1(L_1-L+x))} + E_2 e^{(ik_2(L_1-L+x))} + F_2 e^{(ik_3(L_1-L+x))} for x \in (0, L-L_1) \\ \overline{\theta_2} &= A_2\beta_1 e^{(-ik_1(L_1+x))} + B_2\beta_2 e^{(-ik_2(L_1+x))} + \in_2 \beta_3 e^{(-ik_3(L_1+x))} + D_2\beta_4 e^{(ik_1(L_1-L+x))} \\ &\quad + E_2\beta_5 e^{(ik_2(L_1-L+x))} + F_2\beta_6 e^{(ik_3(L_1-L+x))} for x \in (0, L-L_1), \end{aligned} \tag{26}$$

Moments and shear forces)

$$
\begin{aligned}
&x = L_1 \ for \ u_1(x), w_1(x), \theta_1(x) \ and \ x = 0 for u_2(x), w_2(x), \theta_2(x)\\
&u_2(x) - u_1(x) - \phi\frac{\partial u_1(x)}{\partial x} = 0\\
&EA\frac{\partial u_1(x)}{\partial x} + C_1\left(\frac{\partial w_1(x)}{\partial x} - \theta_1(x)\right) + C_2\frac{\partial \theta_1(x)}{\partial x} - \left(EA\frac{\partial u_2(x)}{\partial x} + C_1\left(\frac{\partial w_2(x)}{\partial x} - \theta_2(x)\right) + C_2\frac{\partial \theta_2(x)}{\partial x}\right) = 0\\
&w_2(x) - w_1(x) - \xi\left(\frac{\partial w_1(x)}{\partial x} - \theta_1(x)\right) = 0\\
&C_1\frac{\partial u_1(x)}{\partial x} + GA\left(\frac{\partial w_1(x)}{\partial x} - \theta_1(x)\right) + C_3\frac{\partial \theta_1(x)}{\partial x} - \left(C_1\frac{\partial u_2(x)}{\partial x} + GA\left(\frac{\partial w_2(x)}{\partial x} - \theta_2(x)\right) + C_3\frac{\partial \theta_2(x)}{\partial x}\right) = 0\\
&\theta_2(x) - \theta_1(x) - \Omega\frac{\partial \theta_1(x)}{\partial x} = 0\\
&C_2\frac{\partial u_1(x)}{\partial x} + C_3\left(\frac{\partial w_1(x)}{\partial x} - \theta_1(x)\right) + EI\frac{\partial \theta_1(x)}{\partial x} - \left(C_2\frac{\partial u_2(x)}{\partial x} + C_3\left(\frac{\partial w_2(x)}{\partial x} - \theta_2(x)\right) + EI\frac{\partial \theta_2(x)}{\partial x}\right) = 0,
\end{aligned}
\tag{29}
$$

where ϕ, ξ, and Ω are the non-dimensional form for the axial, bending, and shear flexibilities, respectively. By considering the formulae describing the nodal spectral displacements in Eqs. (27) - (29) for the left and right parts of the Timoshenko beam, the boundary conditions in the form of a matrix are expressed as

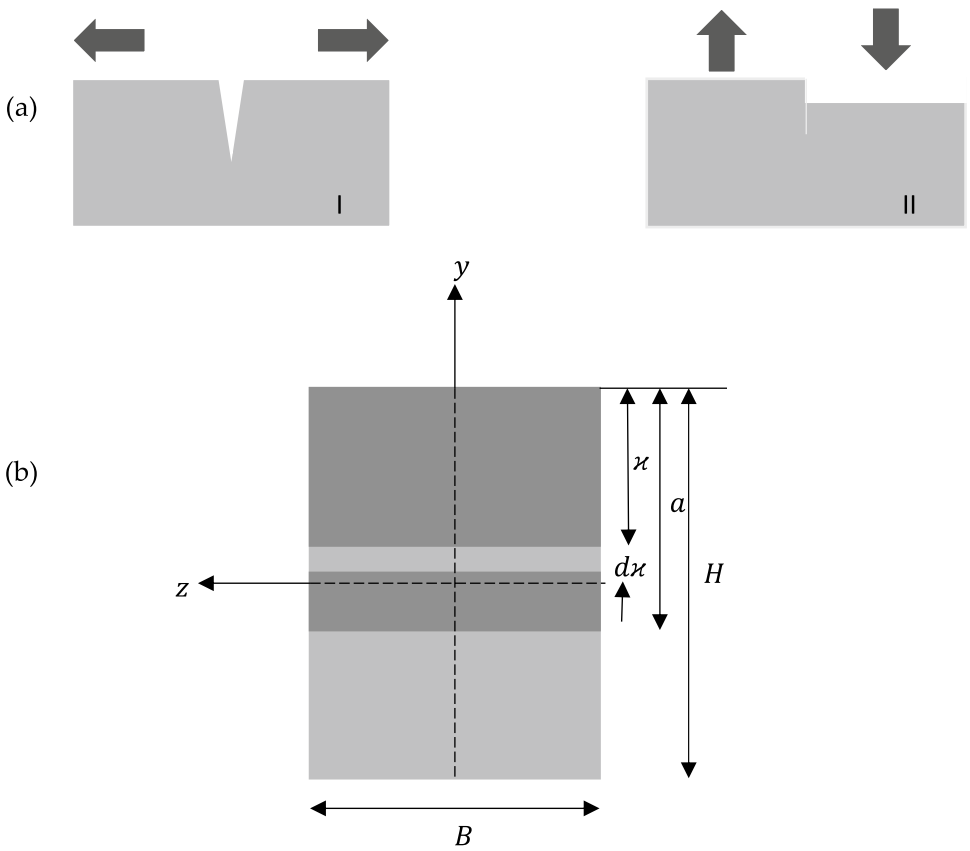

Fig. 5 Flexibility at the crack location: **a** first (I) and second (II) crack propagation modes; **b** cross-section of beam element at the crack location

$$\left[cT_1\right]_{12\times12}\begin{bmatrix} A_1 \\ B_1 \\ \in_1 \\ D_1 \\ . \\ . \\ \in_2 \\ D_2 \\ E_2 \\ F_2 \end{bmatrix}_{12\times1} = \begin{bmatrix} q_1 \\ q_2 \\ q_3 \\ q_4 \\ q_5 \\ q_6 \\ 0 \\ . \\ . \\ 0 \end{bmatrix}_{12\times1} . \tag{30}$$

The nodal spectral forces (P- axial force, T- shear force, and M- bending moment) are obtained by differentiating the spectral displacements; and formerly written in the matrix system as

$$\left[cT_2\right]_{6\times12}\begin{bmatrix} A_1 \\ B_1 \\ \in_1 \\ D_1 \\ . \\ . \\ \in_2 \\ D_2 \\ E_2 \\ F_2 \end{bmatrix}_{12\times1} = \begin{bmatrix} P_1 \\ V_1 \\ M_1 \\ P_2 \\ V_2 \\ M_2 \end{bmatrix}_{6\times1} . \tag{31}$$

From $\left[\boldsymbol{cT}_1\right]$ and $\left[\boldsymbol{cT}_2\right]$, the square matrix (6×6), which signifies the frequency-dependent dynamic stiffness for a coupled axial-bending Timoshenko beam spectral element with transverse open and non-propagating crack, is obtained. It is represented in the Appendix section; refer to Equation (A7) and Equation (A8).

Flexibilities in a Crack Region

The beam flexibilities at the crack region are obtained from Castigliano's theorem by the following equation:

$$c_{ij} = \frac{\partial^2 U}{\partial P_i \partial P_j} i = 1, 2, ..6, j = 1, 2, ..6, \tag{32}$$

where U represents the elastic strain energy of the element caused by the presence of the crack, and P is an independent nodal force acting on the element. The elastic strain energy due to the crack is expressed as [43]

$$U = \frac{1}{E}\int_{A_a}\left(K_I^2 + K_{II}^2\right)dA_a, \tag{33}$$

where K_I and K_{II} denote stress intensity factors corresponding to the first and second crack growth mode, and A_a denotes crack area. Figure 5 shows the first (I) and second (II) crack propagation modes and cross-section of beam element at the crack location.

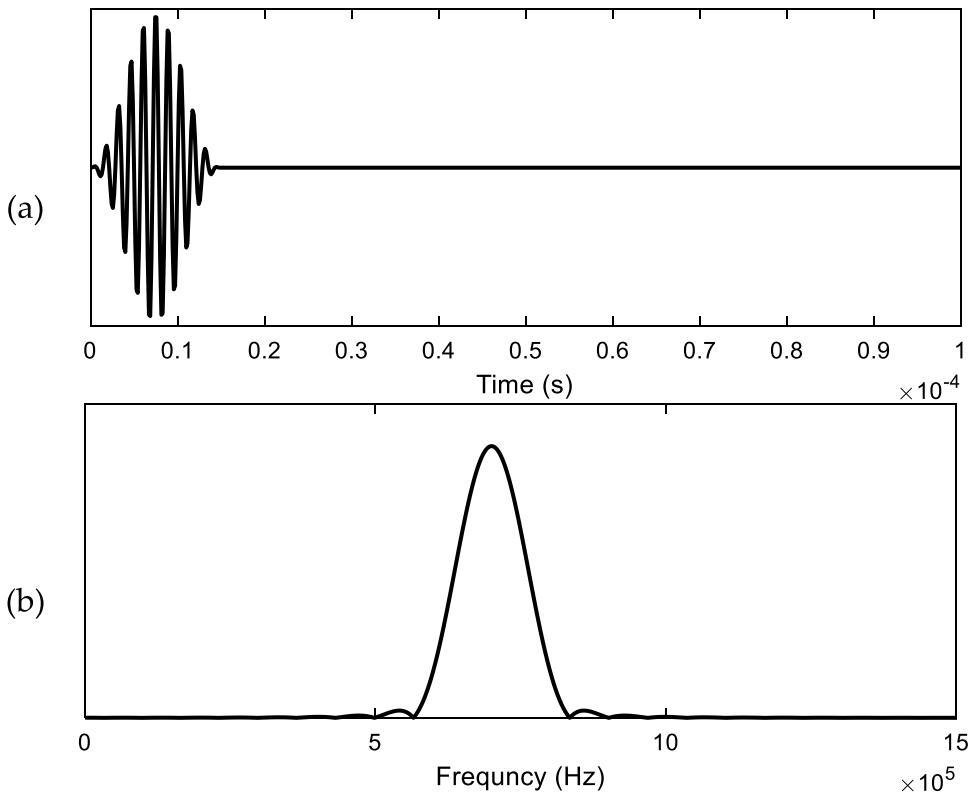

Fig. 6 Excitation signal in **a** time domain and **b** frequency domain

Axial Flexibility

The stress intensity factor corresponding with the first mode of the crack formation due to the load P_1 is obtained as

$$K_a = \frac{P_1}{A_a}\sqrt{\pi \varkappa} F_I\left(\frac{\varkappa}{H}\right), \tag{34}$$

where $\varkappa$ and H are illustrated in Fig. 5 (b). F_I is the correction factor expressed as [37]

$$F_I\left(\frac{\varkappa}{H}\right) = \sqrt{\frac{tan(\pi\varkappa/2H)}{\pi\varkappa/2H}}\frac{0.752 + 2.02(\varkappa/H) + 0.37[1 - sin(\pi\varkappa/2H)]^3}{cos(\pi\varkappa/2H)}. \tag{35}$$

The flexibility of the elastic element modeling of the cracked cross-section of the rod spectral finite element is rewritten as

$$c_a = \frac{2\pi(1-\nu^2)}{EB}\int_0^{\bar{a}} \overline{\varkappa} \mathrm{F}_I^2(\overline{\varkappa}) d\overline{a} \tag{36}$$

$$\phi = EA_a c_a,$$

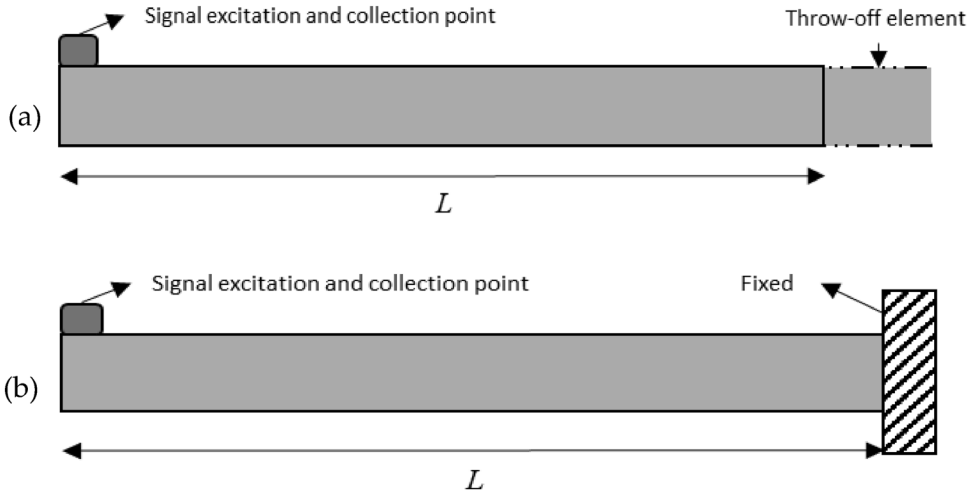

Fig. 7 Proposed Timoshenko beam model: **a** for Test-I and **b** for Test-II, respectively

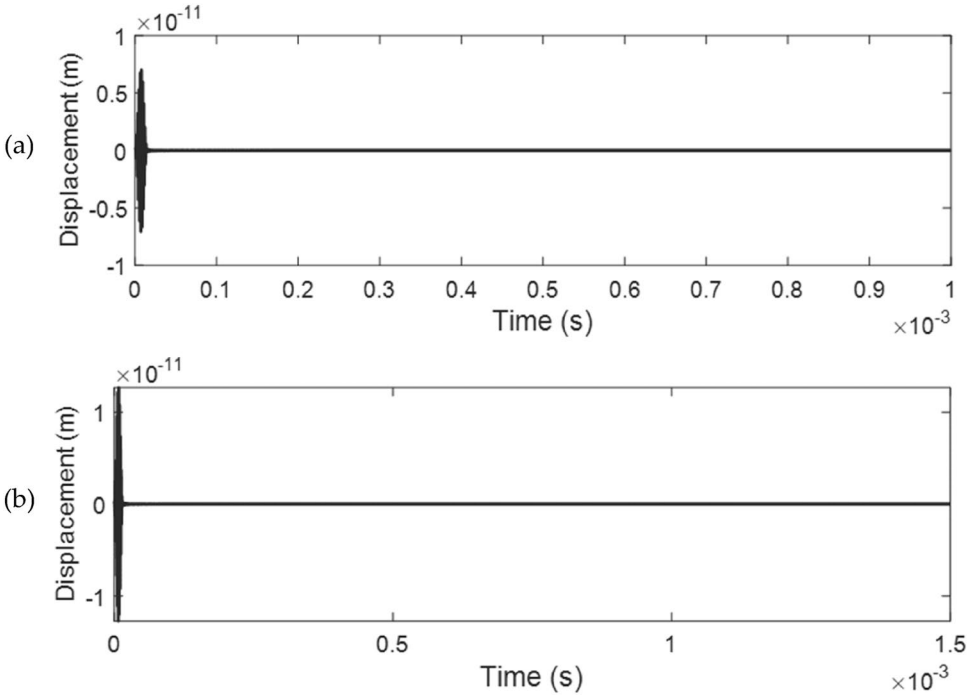

Fig. 8 Wave propagation in Test-I for **a** axial and **b** bending parts

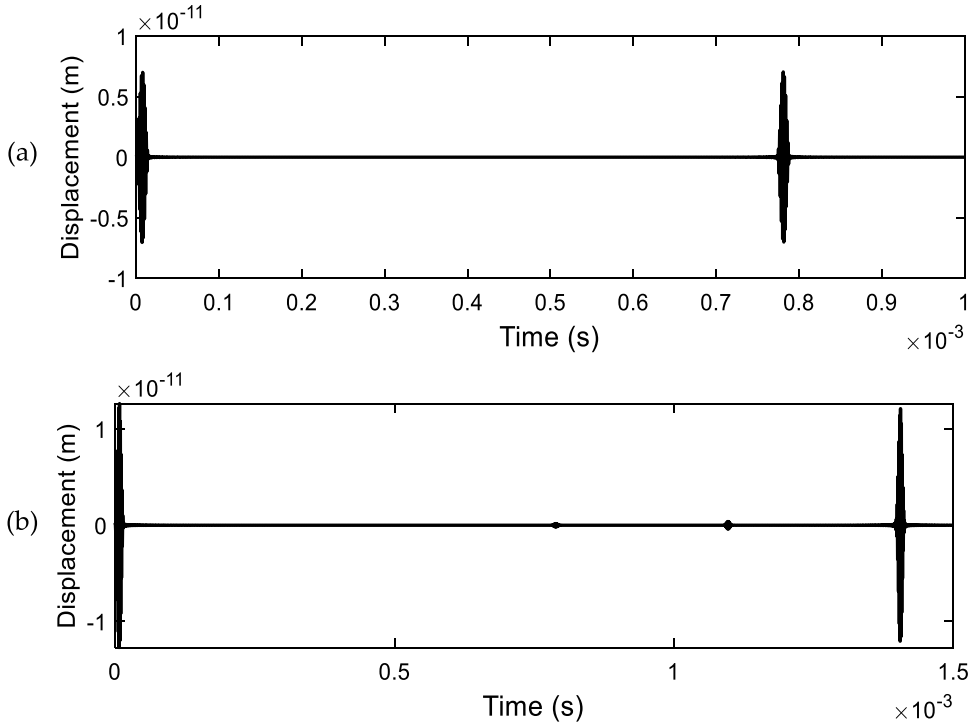

Fig. 9 Wave propagation in Test-II for **a** axial and **b** bending parts, respectively

where c_a is the axial flexibility due to the presence of a crack; $\overline{a} = \frac{a}{H}$ and $\overline{\varkappa} = \frac{\varkappa}{H}$; ϕ is the non-dimensional form of axial flexibilityc_a; $A_a = BH$ (refer to Fig. 5).

Bending Flexibility

Similar to the axial flexibility, the stress intensity factors due to the bending moment M and shear force V are obtained as

$$K_I = \frac{6M}{BH^2}\sqrt{\pi\varkappa}F_I\left(\frac{\varkappa}{H}\right), K_{II} = \frac{\vartheta V}{BH}\sqrt{\pi\varkappa}F_{II}\left(\frac{\varkappa}{H}\right), \tag{37}$$

where ϑ is the shear factor [44]; F_{I} (refer to Eq. (35)) and F_{II} are correction functions expressed as

$$F_{II}\left(\frac{\varkappa}{H}\right) = \frac{1.30 - 0.65(\varkappa/H) + 0.37(\varkappa/H)^2 + 0.28(\varkappa/H)^3}{\sqrt{1-(\varkappa/H)}}. \tag{38}$$

The modeling of the flexibilities of the elastic elements cracked cross-section of a coupled axial-bending Timoshenko beam finite spectral element is written as

$$c_b = \frac{72\pi(1-\nu^2)}{BH^2E}\int_0^{\overline{a}} \overline{\varkappa}F_I^2(\overline{\varkappa})d\overline{a}, c_s = \frac{4\vartheta\pi(1-\nu^2)}{BE}\int_0^{\overline{a}} \overline{\varkappa}F_{II}^2(\overline{\varkappa})d\overline{a}$$

$$\xi = \frac{EIc_b}{L}, \Omega = \frac{GA_ac_s}{L}, \tag{39}$$

where c_b and c_s denote bending and shear flexibilities, respectively; $\overline{a} = \frac{a}{H}$ and $\overline{\varkappa} = \frac{\varkappa}{H}$ (refer to Fig. 5); ξ and Ω are the non-dimensional form for the bending and shear flexibilities, respectively.

Numerical Investigations

Several numerical investigations have been performed to demonstrate the effectiveness of the proposed model on beams. Figure 6 shows the input excitation signal in the time domain and its FFT in the frequency domain. The beam has dimensions of 2.0 m in length, 0.02 m in height, and 0.02 m in width; Young's modulus is 210 GPa, and a mass density of 7860 kg/m^3 is considered for the analysis. The beam model is excited by a signal of 0.7 MHz. It is the product of a Hanning window lasting for 125 μs, performed through convolution in the frequency domain, which distributes the effects of the pulse. It is understood that a signal that lasts for a short time can excite a wider range of frequencies in the frequency domain for the tested signal. The dynamic stiffness matrix derived for coupled axial-bending cracked Timoshenko beam in Eqs. (30) and (31) is used for numerical investigations.

The first and second numerical tests validate the proposed Timoshenko beam model for capturing forward and backward moving waves. All the coupling coefficients are considered zero ($C_1, C_2, C_3 = 0$), and the first moment of

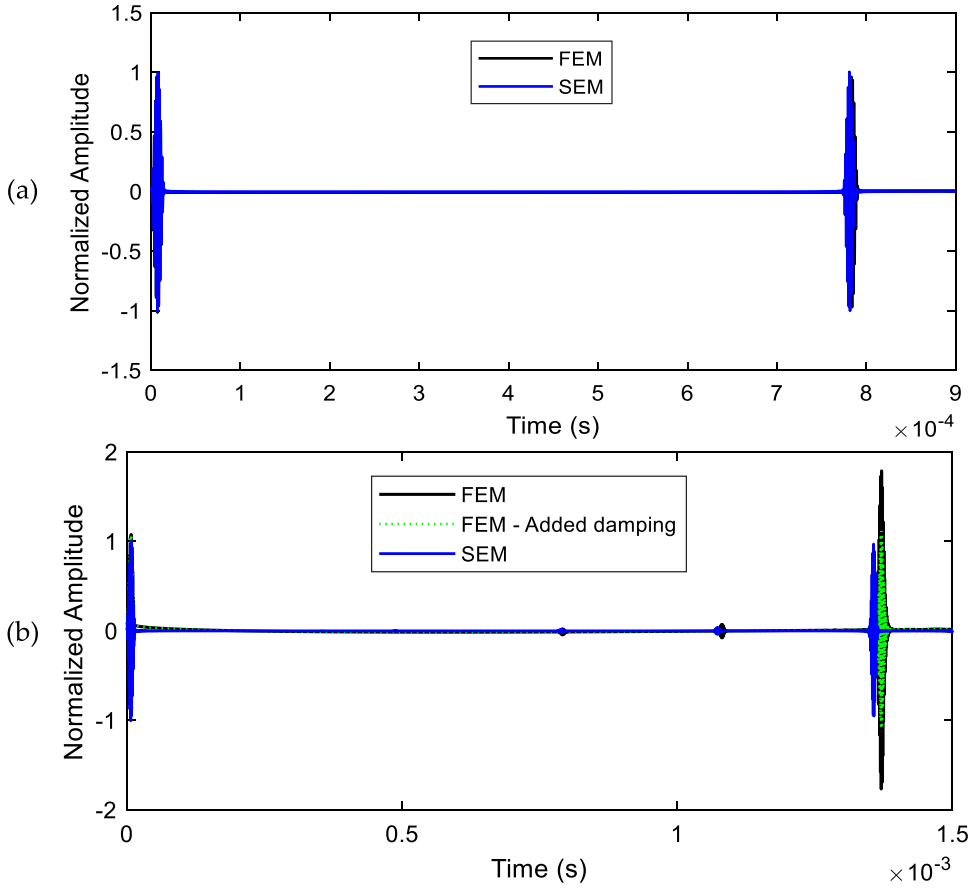

Fig. 10 **a** Wave propagation in Test-II for **a** axial and **b** bending parts, respectively, compared with FEM

inertia is also zero ($\rho R = 0$). Figure 7 (a) shows that the first numerical test model (Test-I) consists of classical Timoshenko beam and throw-off elements with the position of measurement points. The second numerical test model (Test-II) consists of only one classical Timoshenko beam element, as shown in Fig. 7 (b). It is exciting from one end, and the other has a fixed boundary condition.

Figure 8 shows the wave propagation for the model in the axial and bending part of the Timoshenko beam, respectively. There is no reflection from the beam's other end due to the throw-off element's presence, as it acts like a conduit that throws the wave energy out of the system. Figure 9 shows the wave propagation for the model in the axial and bending part of the Timoshenko beam, respectively. There is a reflection from the fixed end, as expected. Thus, both numerical tests show that the model can capture forward and backward propagating waves. From the reasons mentioned above, it can be seen that with the proposed spectral Timoshenko beam element with a crack, the dynamically changing stiffness matrix can be obtained without any additional mathematical computation. In this figure, these are the reflections of the second mode of bending part of coupled axial-bending Timoshenko beam. Coupled axial-bending Timoshenko beam is a higher order beam theory. The bending part of coupled axial-bending Timoshenko beam has two modes. In paper $k_2(\omega)$ and $k_3(\omega)$. $k_2(\omega)$ is always real, and $k_3(\omega)$ is initially imaginary, but it also becomes real after crossing the cut-off frequency. The excitation frequency in this paper is beyond the cut-off frequency; hence, the second mode propagates. Compared to the Euler–Bernoulli beam, it also has two modes, but the second mode is equal to the first mode and always imaginary, hence no propagation. The wave propagation in structures depends upon the material and cross-sectional properties. The axial and bending waves have different propagating speeds. The axial wave propagation speed is equal to $\sqrt{\frac{E}{\rho}}$.

In contrast, in the Timoshenko beam, the expression for group speed is more complex and frequency-dependent, and the speed is slower than the axial part. The axial part has only one propagating mode, which is not observed in the axial part. Only the bending part has a reflection of the first and second modes from the crack.

The third numerical test model (Test-III) illustrates the influence of the presence of a crack in the beam, as shown in Fig. 10a. The crack introduced is a transverse open and non-propagating crack. It is located at 25% of the beam length, and the crack depth is 15% of the beam depth. The proposed beam model is excited with the input signal, as shown in Fig. 7. All the coupling coefficients are

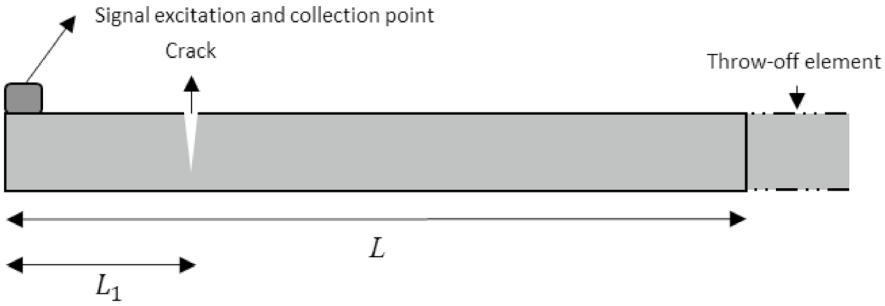

(a) Proposed beam model for numerical Test-III with crack.

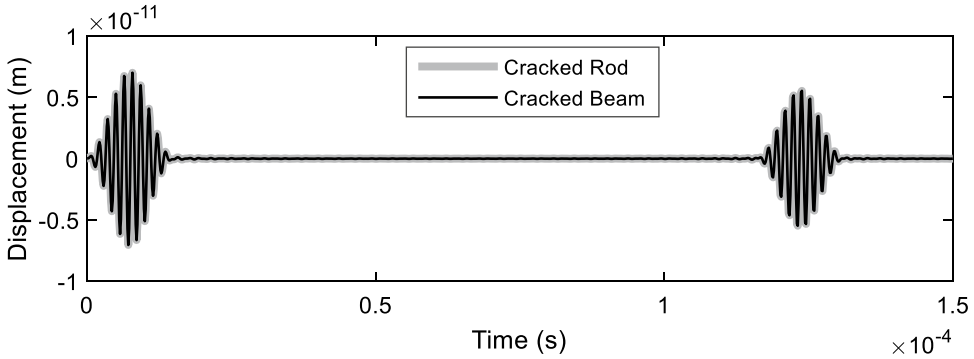

(b) for axial part

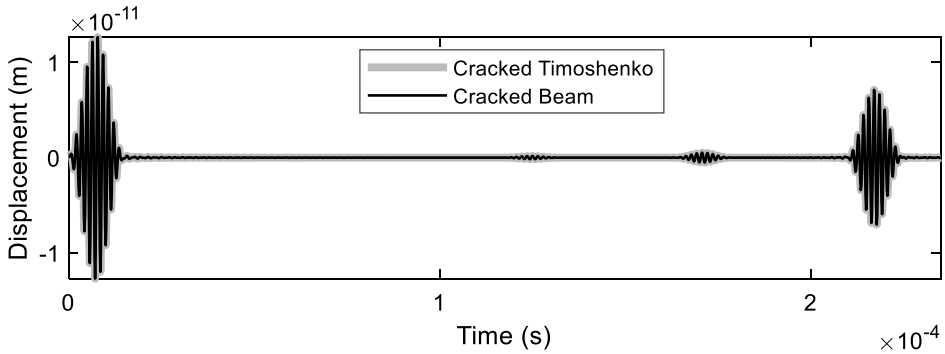

(c) for bending part

Fig. 11 Dynamic stiffness for axial degree of freedom at **a** low frequency and **b** high frequency

considered zero ($C_1, C_2, C_3 = 0$), and the first moment of inertia is also taken as zero ($\rho R = 0$). The model consists of one cracked Timoshenko beam element in the middle and two throw-off elements at both ends. The results are compared in Fig. 10 (b) and 10 (c), with a cracked rod for the axial part [35] and a cracked Timoshenko beam for the bending part [36].

Figure 10b shows that the first wave packet stands for the excitation signal, and the second is reflected from the crack. There is no third reflection as it is a throw-off spectral element. The Timoshenko beam axial response agrees with the cracked rod results. Likewise, the Timoshenko beam bending response closely matches the cracked Timoshenko beam model.

To validate the wave propagation results obtained above, tests were also carried out in the time domain (FEM). The lack of throw-off elements makes it challenging to analyze when both forward and moving waves are present. Therefore, infinite boundary conditions are difficult to implement. Therefore, semi-infinite beam is not modeled in FEM.

Wave reflection from a fixed boundary condition is performed in FEM and compared with the SEM in Fig. 10. To perform this analysis, 1000 elements in 2 m were discretized. The time step was very small equal to 1.5e-8 s. Compared to SEM, to obtain the same results, only one element is required, and the analysis is not required for the whole range; since the beam is excited at 700 kHz, a band around that specific frequency is enough. This also saves lots of computation cost for integrations making it faster than

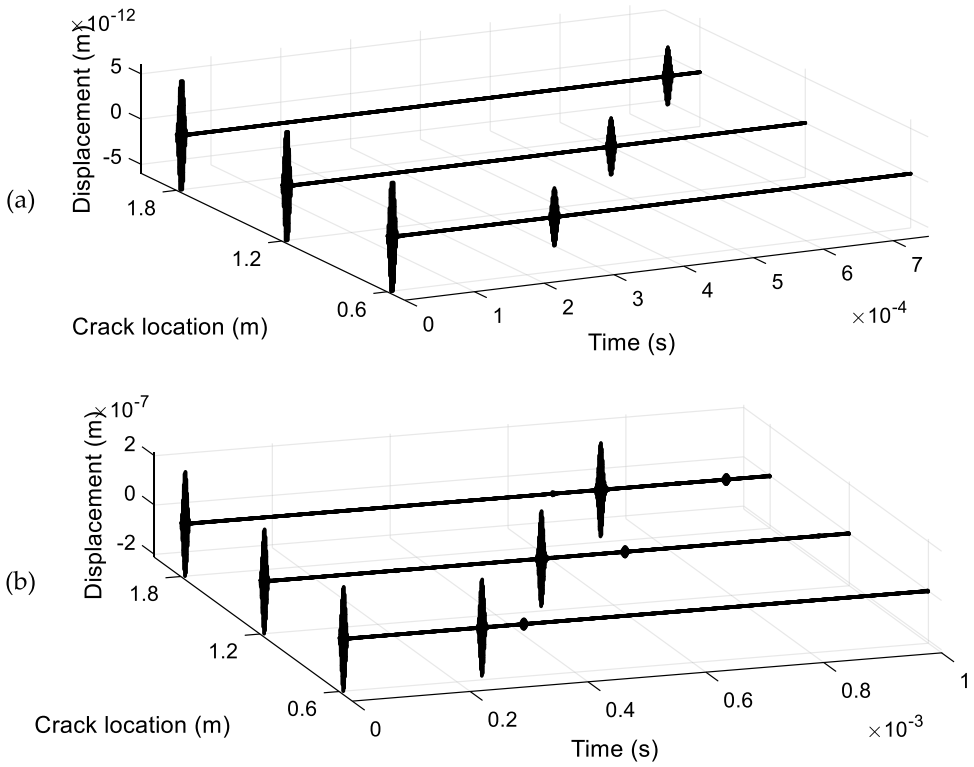

Fig. 12 Reflection from element representing a crack in simple bar element

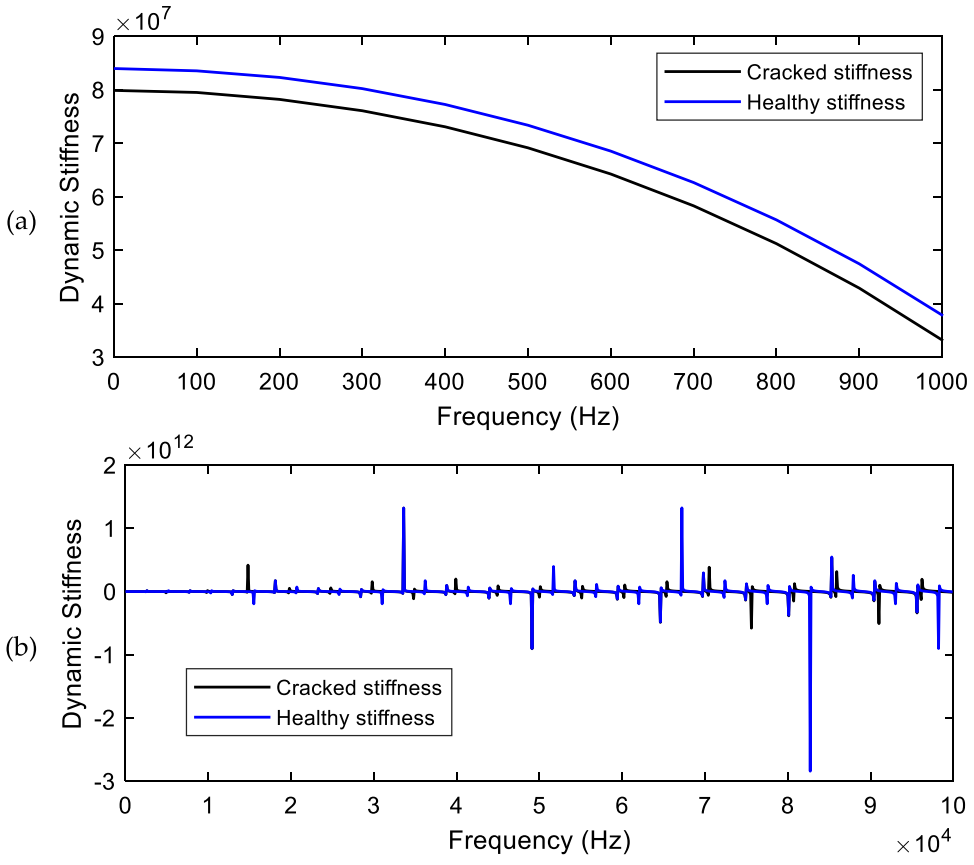

Fig. 13 Proposed beam model for numerical Test-III and its wave propagation phenomenon

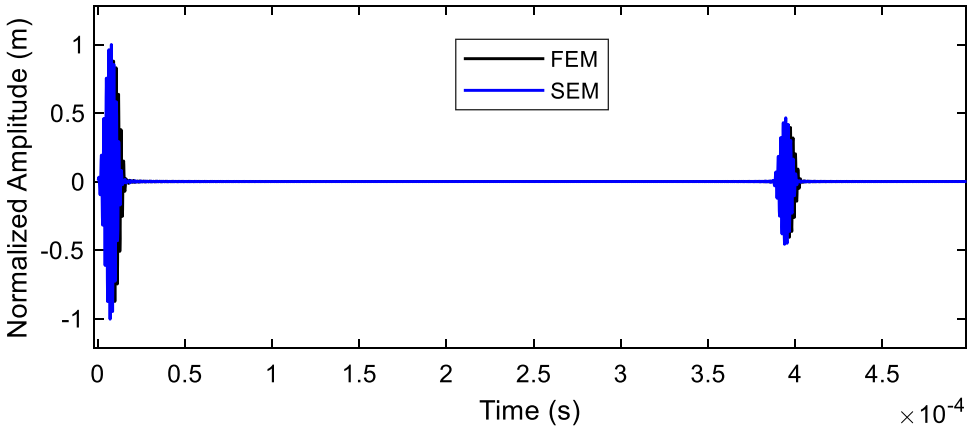

Fig. 14 Influence of varying crack position on the wave propagation in beam for **a** axial part and **b** bending part, respectively

Table 1 Properties of a coupled axial-bending Timoshenko beam model with coupling coefficients

$EA = 8.4\text{x}10^7 N$	$GA = 3\text{x}10^7 N$	$EI = 2.8\text{x}10^7 Nm^2$
$C_1 = 0Nm$	$C_2 = -1.68\text{x}10^7 Nm$	$C_3 = 0Nm$
$\rho A = 3.144 kg/m$	$\rho R = 0kg$	$\rho I = 1.05\text{x}10^{-4} kgm$

FEM. From this analysis, it is evident that SEM is advantageous over FEM for high-frequency analysis. As shown in Fig. 10b, the results were distorted and exploded at the end. This result was obtained without adding any damping in an explicit time integration scheme. This is a disadvantage in the time domain as the same result is obtained accurately using SEM when no damping is applied. When a small damping is applied to the explicit scheme to make it stable, the reflections of the second propagating mode (higher frequency mode) disappear, as shown in Fig. 10b. This shows another advantage of SEM that it can do theoretical simulations when there is no damping. The explicit time domain is sensitive to two things: a) CFL condition and b) absence of damping in the model leads to inherent instability.

Modeling the same crack in the conventional FEA software has the following challenges: (a) stiffness of the crack is frequency-dependent, (b) non-orthogonal due to the equation of coupled axial-bending wave propagation, and (c) coupled to other degrees of freedom. Figure 11 shows the variation of dynamic stiffness of axial degree of freedom of axial-bending coupled Timoshenko beam with respect to the frequency at low and high frequencies. Figure shows stiffness reduction when the crack (a/H = 0.5) is present.

To validate the results for wave propagation in FEM and SEM, the following workaround is proposed to validate wave propagation in axial direction. In FEM, the crack is modeled as tiny element, whose stiffness is obtained from the dynamic stiffness matrix of SEM element at low frequency corresponding to the axial degree of freedom. The results obtained are shown in Fig. 12. The time taken for the wave to return is half the time to reflect from the boundary for the axial part of coupled axial-bending Timoshenko beam.

The influences of varying crack locations on the wave propagation in the beam for axial and bending parts are presented in Fig. 14a, b, respectively. The location of the crack is changed to find out how the model will behave when the location of the crack moves away from the excitation node. Correspondingly, Figs. 13c and 14b show the presence of a second propagating mode [10], which is faster than the first mode.

The fourth and fifth numerical tests are examined to show that the proposed coupled axial-bending cracked Timoshenko beam model is useful for modal analysis. For the free-vibration analysis, the model is considered without coupling coefficients (Test-IV) and with coupling coefficients (Test-V). The investigation is carried out on the beam

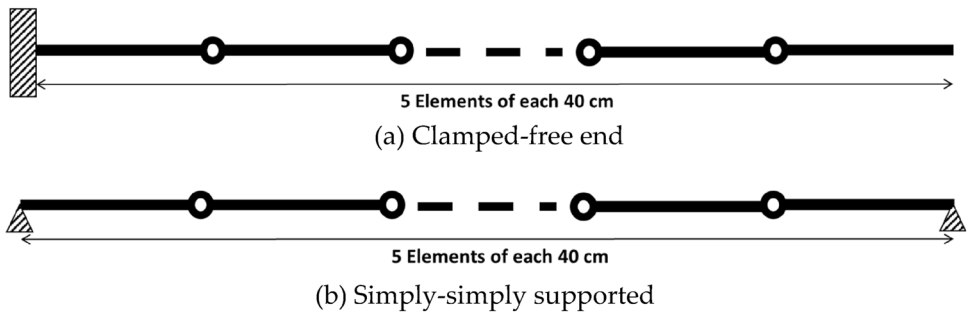

Fig. 15 Proposed beam models with different boundary conditions utilized for Tests-IV and V

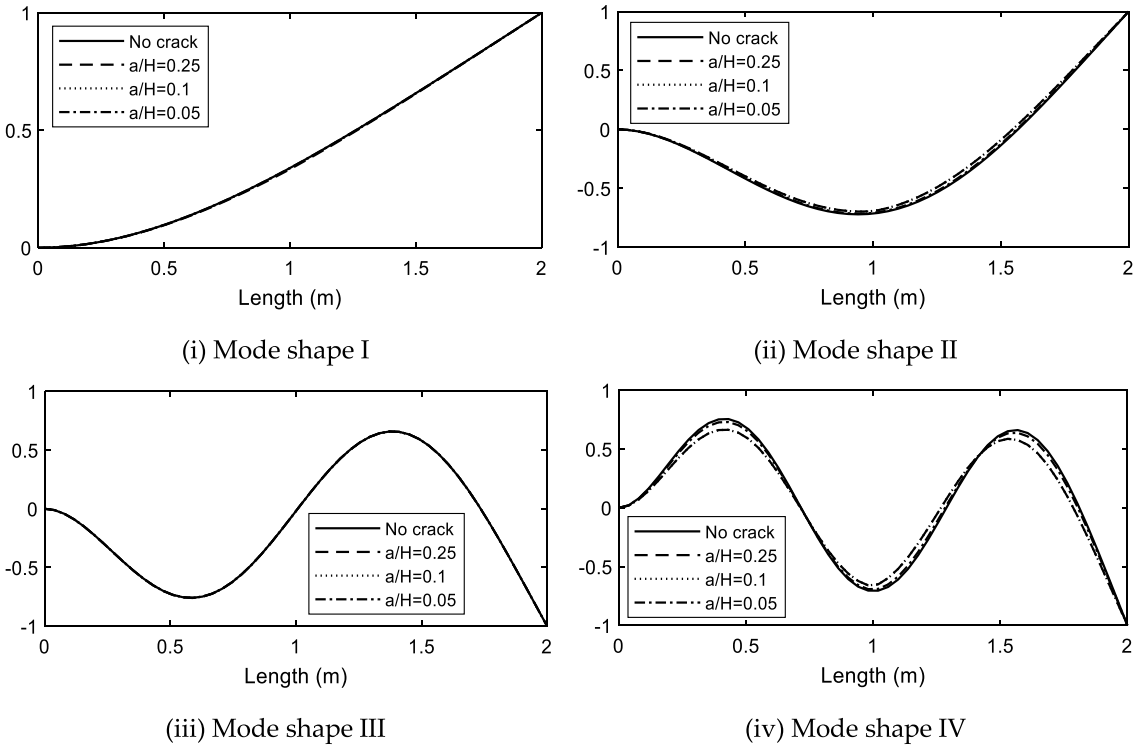

(i) Mode shape I (ii) Mode shape II

(iii) Mode shape III (iv) Mode shape IV

(a) for the clamped-free beam

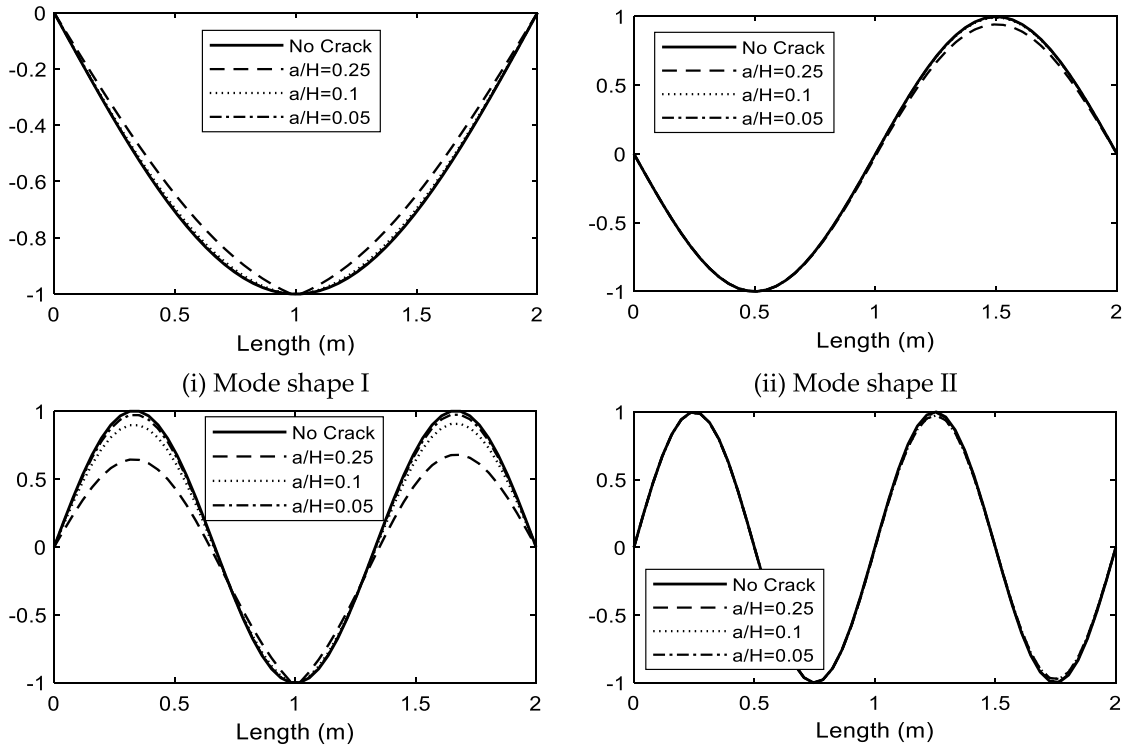

(i) Mode shape I (ii) Mode shape II

(iii) Mode shape III (iv) Mode shape IV

(b) for the simply supported beam

Fig. 16 Lowest four bending normal modes without coupling effects

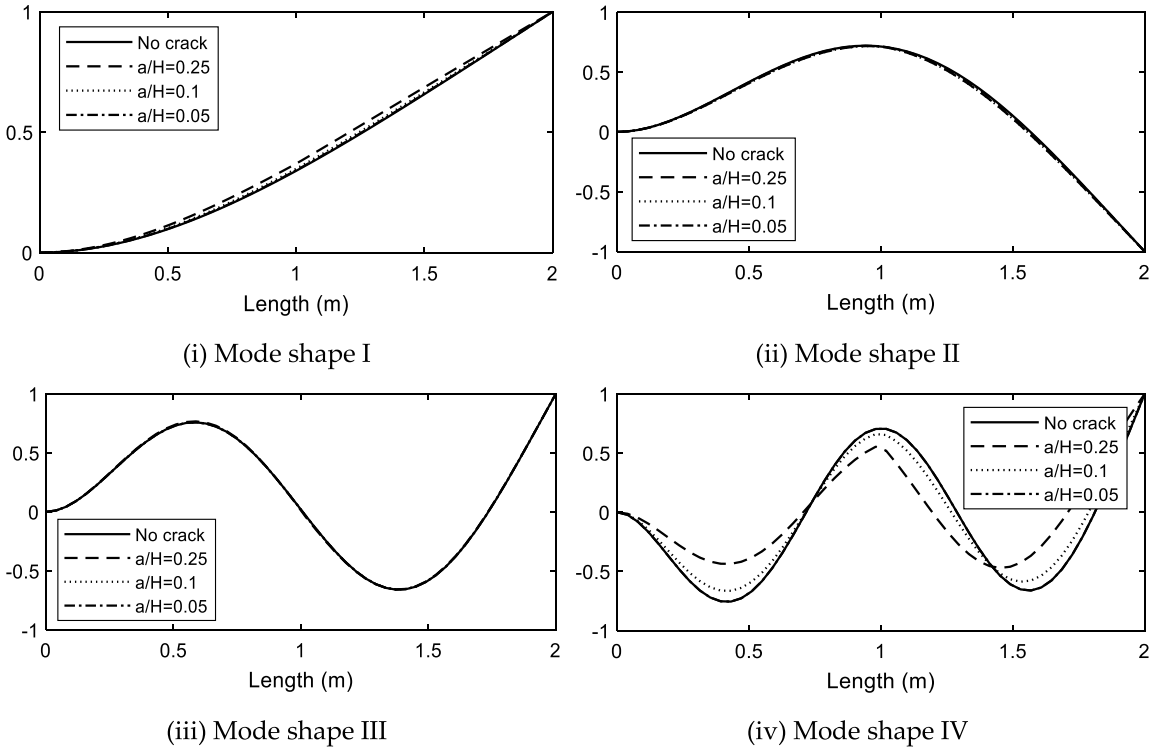

(i) Mode shape I (ii) Mode shape II

(iii) Mode shape III (iv) Mode shape IV

(a) for the clamped-free beam

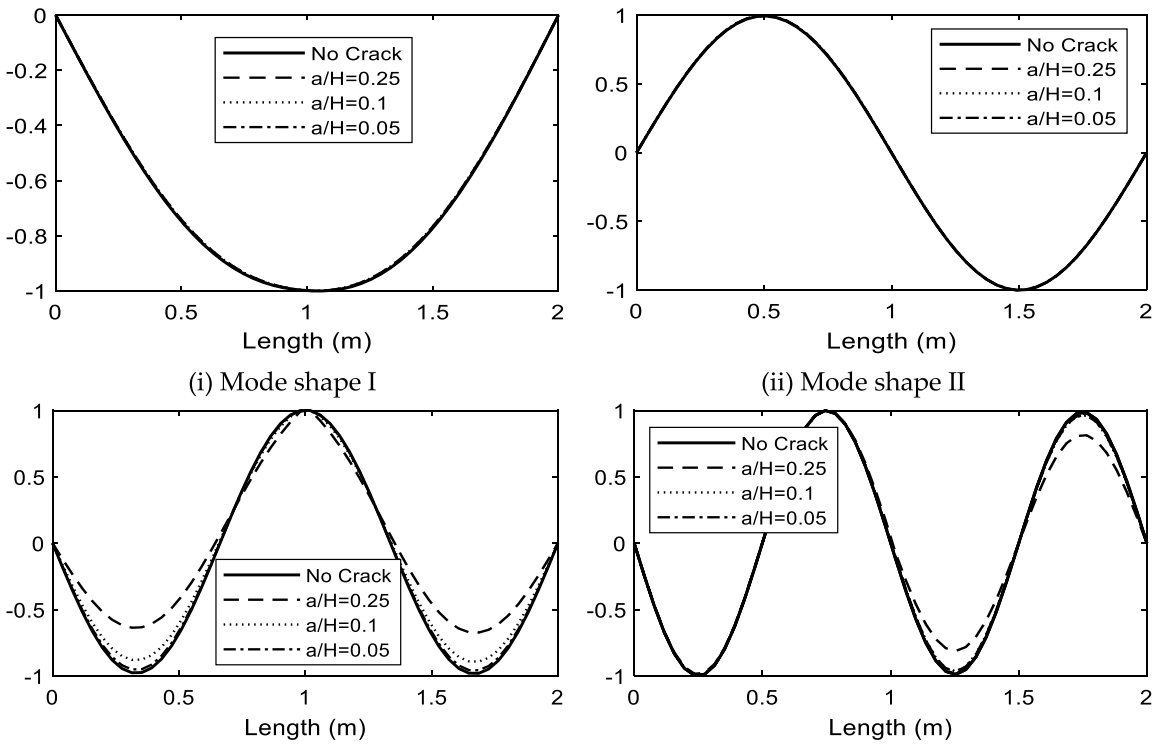

(i) Mode shape I (ii) Mode shape II

(iii) Mode shape III (iv) Mode shape IV

(b) for the simply supported beam

Fig. 17 Lowest four bending normal modes for the simply supported beam with coupling effects

Table 2 Estimated natural frequencies for the clamped-free beam with various crack formations

Natural frequencies (rad/s)	Relative crack depth				
	No crack	$\frac{a}{H}$= 0.05	$\frac{a}{H}$= 0.1	$\frac{a}{H}$= 0.25	$\frac{a}{H}$= 0.5
Without coupling effect					
Frequency I	26.20	26.20	26.20	26.14	25.76
Frequency II	164.24	164.18	164.05	162.79	153.06
Frequency III	459.68	459.68	459.68	459.68	459.68
Frequency IV	899.88	899.69	898.93	892.40	845.84
With coupling effect					
Frequency I	24.57	24.69	24.94	26.70	31.23
Frequency II	154.01	154.06	154.19	155.15	161.86
Frequency III	431.28	431.22	431.22	431.22	431.28
Frequency IV	844.15	843.89	843.20	836.98	792.94

Table 3 Estimated natural frequencies for the simply–simply supported beam with various crack formations

Natural frequencies (rad/s)	Relative crack depth				
	No crack	$\frac{a}{H}$= 0.05	$\frac{a}{H}$= 0.1	$\frac{a}{H}$= 0.25	$\frac{a}{H}$= 0.5
Without coupling effect					
Frequency I	11.72	11.72	11.71	11.62	10.91
Frequency II	46.85	46.85	46.85	46.85	46.85
Frequency III	105.33	105.30	105.21	104.44	98.83
Frequency IV	187.04	187.04	187.04	187.04	187.04
With coupling effect					
Frequency I	20.56	20.56	20.56	20.55	20.47
Frequency II	43.93	43.93	43.93	43.93	43.93
Frequency III	99.71	99.68	99.61	98.94	94.08
Frequency IV	175.42	175.42	175.42	175.42	175.42

Table 4 Comparison of natural frequencies for clamped-free and without coupling effects

Natural frequency (Rad/s)	No Crack		a/H = 0.05		a/H = 0.25		a/H = 0.5	
	Present	M. Krawczuk et. al [42]	Present	M. Krawczuk et. al [42]	Present	M. Krawczuk et. al [42]	Present	M. Krawczuk et. al [42]
Frequency I	26.2	26.138	26.2	26.138	26.14	26.138	25.76	25.887
Frequency II	164.24	164.24	164.18	164.24	162.79	163.36	153.06	157.21
Frequency III	459.68	459.62	459.68	459.62	459.68	456.62	459.68	459.62
Frequency IV	899.88	899.75	899.69	899.63	892.4	895.23	845.84	864.5

models, namely, clamped-free and simply–simply supported boundary conditions, with and without crack, to estimate modal properties. Table 1 illustrates the structural properties of the beam model with coupling coefficients. The proposed spectral elements are used in a planar beam with five repeating elements (i.e., 2 m overall length) to assess the natural frequency when exposed to different boundary conditions. The length of the repeating element unit is 40 cm. Figure 15 illustrates the beam model in clamped-free and simply–simply supported boundary conditions.

For the numerical Tests-IV and V, the beam models are considered without and with coupling effects, respectively. The crack is located in the middle of the beam model. The parametric study is conducted for modal analysis to understand the crack depth effect by varying it from 5 to 25% of the beam height ($\frac{a}{H}$ ratio). The natural frequencies for both support conditions are calculated using the STMM for all the crack depths. The beam model is excited with the respective natural frequencies. Figure 16a, b shows the first four normal bending mode shapes of the beam model without

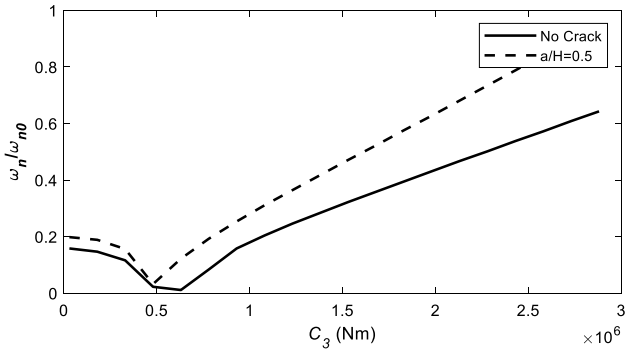

(a) clamped-free beam

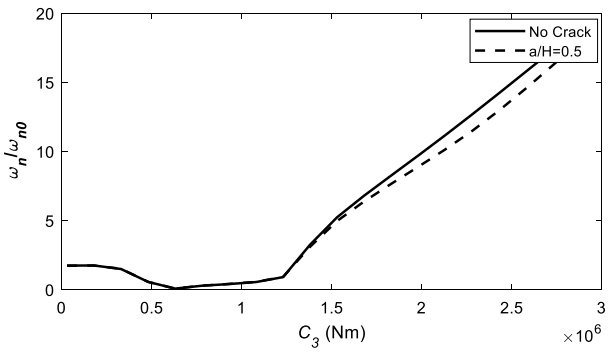

(b) simply supported beam

Fig. 18 Variation of ω_n/ω_{n0} with the C_3 value

coupling effects for clamped-free and simply–simply supported boundary conditions, respectively.

The investigation for Test-V is executed with a shear-bending coupling coefficient (C_3) taken into account. Figure 17a, b shows the first four normal bending mode shapes of the beam model with coupling effects for clamped-free and simply–simply supported boundary conditions, respectively. The computed natural frequency results considering coupling effects with varying crack depths are tabulated for beam models with clamped-free and simply–simply supported boundary conditions in Tables 2 and 3. The results are validated and found to agree with the values presented in Ref. [42] for the non-coupling and clamped-free part. Table 4 summarizes and compare with ref. [42] for SEM.

The numerical tests are investigated to show that the proposed element works fine and is verified with various parameters. The flexibility at the crack locations and beam with a coupling coefficient is also explained well. It is observed that these coupling coefficients are essential for the coupled axial-bending Timoshenko beam element, and the influence of coupling on an overall response needs to be understood in detail. For this, a parametric study is carried out by varying the coefficient value to observe its effects on the overall structural response of the element in its fundamental mode. As the varying coupling coefficients change the element's mode shapes, it directly influences the overall response of the beam. The same material properties explained in Table 1 are used for the parametric study. Tests-I and II are investigated with varying

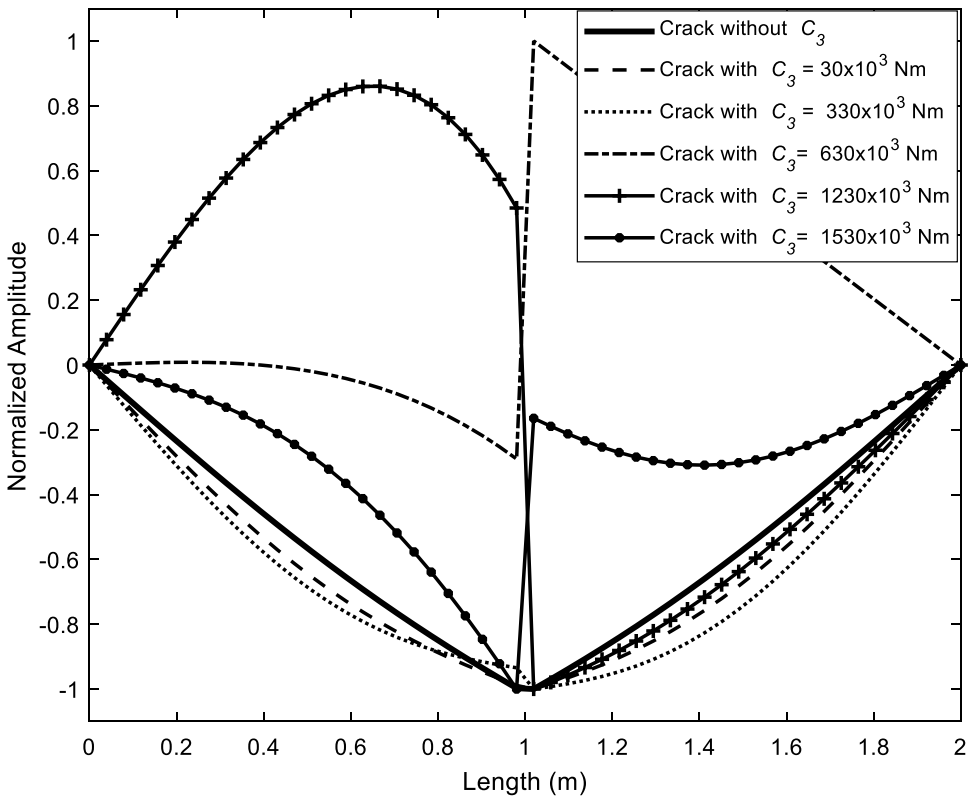

Fig. 19 Mode shape comparison for a simply supported beam with crack

C_3 value for clamped-free and simply supported beams. The crack is located at the mid-span of the beam, and the crack depth is considered half of the beam's depth. Figure 18 (a) and 18 (b) shows the variation of first natural frequencies with the change in C_3 for clamped-free and simply supported beams, respectively. Here, ω_n and ω_{n0} are the natural frequency of the beam without and with crack and coupling effect, respectively.

The ratio (ω_n/ω_{n0}) first decreases and increases for higher C_3 values. At first, there is a slight discontinuity at the mid-span of the beam due to the presence of a crack. As C_3 is increased, the shear deformation is also increased. Since the transverse crack deformation will be very high, all the discontinuities focus on the crack location. This beam behaves in dual nature: one part being a cantilever and the other being supported and connected by the crack. Hence, the beam will not bend; it becomes straight. Therefore, more shear deformation is observed than bending deformation. A few mode shapes are shown in Fig. 19 to display the difference in mode shape in the absence and presence of coupling coefficients.

Conclusions

This paper presents a novel spectral element model for the coupled axial-bending cracked Timoshenko beam element. The work attempts to unify the theory of the SFEM for Timoshenko beam and fracture mechanics in the frequency domain, making it simpler for wave propagation and modal analysis with the presence of coupled axial-bending effects. It is easy to see that the spectral approach provides more information and is more appropriate for detecting damage. The results show that the current approach can calculate higher natural frequencies without additional computational time. An open non-propagating transverse-single edge crack opening is examined in the present research. The inferences derived from the five numerical test investigations are given below:

- Tests-I and II are conducted to investigate whether the coupled axial-bending Timoshenko beam element and the throw-off element are capable of wave propagation as intended. For these numerical models, all the coupling coefficients and the first moment of inertia were set to zero for minimal complications. It is concluded from the investigations that the element allow both forward and backward wave propagation. Test-II was also analyzed in FEM and it showed the few of the many advantages of SEM over FEM in high-frequency analysis.
- In Test-III, the variation in wave propagation analysis is studied in the presence of crack by comparing responses from damaged and undamaged coupled axial-bending Timoshenko beams without coupling coefficients. Then, the effect of crack depth and location is studied for the various wave propagation phenomena. Due to challenges of modeling crack in FEM, to validate wave propagation, analysis for axial degree of freedom was performed. The results were compared for SEM and FEM.
- The modal analyses are carried out in Tests-IV and V on the beam models to obtain natural frequencies and mode shapes to understand the variation of the coupling coefficient (C_3) for crack formation. The natural frequencies for both support conditions are calculated using the STMM for all the crack depths.
- A parametric study is carried out by varying the coefficient value to observe its effects on the overall structural response of the element in its fundamental mode. The ratio (ω_n/ω_{n0}) is well understood for varying C_3 values and the mode shapes are compared for a simply supported beam with a crack present.

The proposed spectral element for the coupled axial-bending cracked Timoshenko beam model has been shown to analyze the damaged structures and precisely identify and evaluate the crack location. Future research will extend the proposed spectral element system to damaged structures of more complex shapes.

Appendix

The dynamic stiffness matrix for a finite length coupled axial-bending Timoshenko beam element is expressed as

$$S(\omega) = \left[T_2\right]\left[T_1\right]^{-1}, \tag{A1}$$

where

$$\left[T_1\right] = \begin{bmatrix} \alpha_1 & \alpha_2 & \alpha_3 & \alpha_4 p_1 & \alpha_5 p_2 & \alpha_6 p_3 \\ 1 & 1 & 1 & p_1 & p_2 & p_3 \\ \beta_1 & \beta_2 & \beta_3 & \beta_4 p_1 & \beta_5 p_2 & \beta_6 p_3 \\ \alpha_1 p_1 & \alpha_2 p_2 & \alpha_3 p_3 & \alpha_4 & \alpha_5 & \alpha_6 \\ p_1 & p_2 & p_3 & 1 & 1 & 1 \\ \beta_1 p_1 & \beta_2 p_2 & \beta_3 p_3 & \beta_4 & \beta_5 & \beta_6 \end{bmatrix} \tag{40}$$

$$\left[T_2\right] = \begin{bmatrix} r_{1,1} & r_{2,2} & r_{3,3} & r_{4,1} p_1 & r_{5,2} p_2 & r_{6,3} p_3 \\ s_{1,1} & s_{2,2} & s_{3,3} & s_{4,1} p_1 & s_{5,2} p_2 & s_{6,3} p_3 \\ t_{1,1} & t_{2,2} & t_{3,3} & t_{4,1} p_1 & t_{5,2} p_2 & t_{6,3} p_3 \\ r_{1,1} p_1 & r_{2,2} p_2 & r_{3,3} p_3 & r_{4,1} & r_{5,2} & r_{6,3} \\ s_{1,1} p_1 & s_{2,2} p_2 & s_{3,3} p_3 & s_{4,1} & s_{5,2} & s_{6,3} \\ t_{1,1} p_1 & t_{2,2} p_2 & t_{3,3} p_3 & t_{4,1} & t_{5,2} & t_{6,3} \end{bmatrix}. \tag{41}$$

The dynamic stiffness matrix for a throw-off coupled axial-bending Timoshenko beam element is expressed as

$$S_{t(\omega)} = \left[T_{t2}\right]\left[T_{t1}\right]^{-1} \tag{42}$$

$$[T_{t1}] = \begin{bmatrix} \alpha_1 & \alpha_2 & \alpha_3 \\ 1 & 1 & 1 \\ \beta_1 & \beta_2 & \beta_3 \end{bmatrix} \tag{43}$$

$$[T_{t2}] = \begin{bmatrix} r_{1,1} & r_{2,2} & r_{3,3} \\ s_{1,1} & s_{2,2} & s_{3,3} \\ t_{1,1} & t_{2,2} & t_{3,3} \end{bmatrix}. \tag{44}$$

$$[T_1] = \begin{bmatrix} \alpha_1 & \alpha_2 & \alpha_3 & \alpha_4 p_1 & \alpha_5 p_2 & \alpha_6 p_3 \\ 1 & 1 & 1 & p_1 & p_2 & p_3 \\ \beta_1 & \beta_2 & \beta_3 & \beta_4 p_1 & \beta_5 p_2 & \beta_6 p_3 \\ \alpha_1 p_1 & \alpha_2 p_2 & \alpha_3 p_3 & \alpha_4 & \alpha_5 & \alpha_6 \\ p_1 & p_2 & p_3 & 1 & 1 & 1 \\ \beta_1 p_1 & \beta_2 p_2 & \beta_3 p_3 & \beta_4 & \beta_5 & \beta_6 \end{bmatrix}$$

The dynamic stiffness matrices for finite length cracked, coupled axial-bending Timoshenko beam elements are expressed as $[\boldsymbol{cT}_1]$ and $[\boldsymbol{cT}_2]$, namely

$$[cT_1] = \begin{bmatrix} \alpha_1 & \alpha_2 & \alpha_3 & \alpha_4 q_1 & \alpha_5 q_2 & \alpha_6 q_3 & 0 & 0 & 0 & 0 & 0 & 0 \\ 1 & 1 & 1 & q_1 & q_2 & q_3 & 0 & 0 & 0 & 0 & 0 & 0 \\ \beta_1 & \beta_2 & \beta_3 & \beta_4 q_1 & \beta_5 q_2 & \beta_6 q_3 & 0 & 0 & 0 & 0 & 0 & 0 \\ 0 & 0 & 0 & 0 & 0 & 0 & \alpha_1 p_1 & \alpha_2 p_2 & \alpha_3 p_3 & \alpha_4 & \alpha_5 & \alpha_6 \\ 0 & 0 & 0 & 0 & 0 & 0 & p_1 & p_1 & p_1 & 1 & 1 & 1 \\ 0 & 0 & 0 & 0 & 0 & 0 & \beta_1 p_1 & \beta_2 p_2 & \beta_3 p_3 & \beta_4 & \beta_5 & \beta_6 \\ f_{1,1} q_1 & f_{2,2} q_2 & f_{3,3} q_3 & g_{4,1} & g_{5,2} & g_{6,3} & \alpha_1 q_1 & \alpha_2 q_2 & \alpha_3 q_3 & \alpha_4 o_1 & \alpha_5 o_2 & \alpha_6 o_3 \\ -r_{1,1} q_1 & -r_{2,2} q_2 & -r_{3,3} q_1 & r_{4,1} & r_{5,2} & r_{6,3} & r_{1,1} q_1 & r_{2,2} q_2 & r_{3,3} q_3 & r_{4,1} o_1 & r_{5,2} o_2 & r_{6,3} o_3 \\ h_{1,1} q_1 & h_{2,2} q_2 & h_{3,3} q_3 & j_{4,1} & j_{5,2} & j_{6,3} & q_1 & q_2 & q_3 & o_1 & o_2 & o_3 \\ -s_{1,1} q_1 & -s_{2,2} q_2 & -s_{3,3} q_3 & s_{4,1} & s_{5,2} & s_{6,3} & s_{1,1} q_1 & s_{2,2} q_2 & s_{3,3} q_3 & s_{4,1} o_1 & s_{5,2} o_2 & s_{6,3} q_3 \\ u_{1,1} q_1 & u_{2,2} q_2 & u_{3,3} q_3 & v_{4,1} & v_{5,2} & v_{6,3} & \beta_1 q_1 & \beta_2 q_2 & \beta_3 q_3 & \beta_4 o_1 & \beta_5 o_2 & \beta_6 o_3 \\ -t_{1,1} q_1 & -t_{2,2} q_2 & -t_{3,3} q_3 & t_{4,1} & t_{5,2} & t_{6,3} & t_{1,1} q_1 & t_{2,2} q_2 & t_{3,3} q_3 & t_{4,1} o_1 & t_{5,2} o_2 & t_{6,3} o_3 \end{bmatrix} \tag{45}$$

$$[cT_2] = \begin{bmatrix} r_{1,1} & r_{2,2} & r_{3,3} & r_{4,1} q_1 & r_{5,2} q_2 & r_{6,3} q_3 & 0 & 0 & 0 & 0 & 0 & 0 \\ s_{1,1} & s_{2,2} & s_{3,3} & s_{4,1} q_1 & s_{5,2} q_2 & s_{6,3} q_3 & 0 & 0 & 0 & 0 & 0 & 0 \\ t_{1,1} & t_{2,2} & t_{3,3} & t_{4,1} q_1 & t_{5,2} q_2 & t_{6,3} q_3 & 0 & 0 & 0 & 0 & 0 & 0 \\ 0 & 0 & 0 & 0 & 0 & 0 & r_{1,1} p_1 & r_{2,2} p_2 & r_{3,3} p_3 & r_{4,1} & r_{5,2} & r_{6,3} \\ 0 & 0 & 0 & 0 & 0 & 0 & s_{1,1} p_1 & s_{2,2} p_2 & s_{3,3} p_2 & s_{4,1} & s_{5,2} & s_{6,3} \\ 0 & 0 & 0 & 0 & 0 & 0 & t_{1,1} p_1 & t_{2,2} p_2 & t_{3,3} p_3 & t_{4,1} & t_{5,2} & t_{6,3} \end{bmatrix}, \tag{46}$$

where

$$\begin{pmatrix} r_{n,m} \\ s_{n,m} \\ t_{n,m} \end{pmatrix} = \begin{bmatrix} C_1 & C_2 & EA \\ GA & C_3 & C_1 \\ C_3 & EI & C_2 \end{bmatrix} \begin{pmatrix} \beta_n + ik_m \\ i\beta_n k_m \\ i\alpha_n k_m \end{pmatrix}$$

$$p_n = e^{-ik_n L} q_n = e^{-ik_n L_1} o_n = e^{-ik_n (L - L_1)}$$

$$f_{n,m} = \left(-1 + i\phi k_m\right)\alpha_n g_{n,m} = \left(-1 - i\phi k_m\right)\alpha_n$$

$$h_{n,m} = -1 + \xi\beta_n + i\xi k_m j_{n,m} = -1 + \xi\beta_n - i\xi k_m$$

$$u_{n,m} = \left(-1 + i\Omega k_m\right)\beta_n v_{n,m} = \left(-1 - i\Omega k_m\right)\beta_n$$

$$[T_2] = \begin{bmatrix} r_{1,1} & r_{2,2} & r_{3,3} & r_{4,1} p_1 & r_{5,2} p_2 & r_{6,3} p_3 \\ s_{1,1} & s_{2,2} & s_{3,3} & s_{4,1} p_1 & s_{5,2} p_2 & s_{6,3} p_3 \\ t_{1,1} & t_{2,2} & t_{3,3} & t_{4,1} p_1 & t_{5,2} p_2 & t_{6,3} p_3 \\ r_{1,1} p_1 & r_{2,2} p_2 & r_{3,3} p_3 & r_{4,1} & r_{5,2} & r_{6,3} \\ s_{1,1} p_1 & s_{2,2} p_2 & s_{3,3} p_3 & s_{4,1} & s_{5,2} & s_{6,3} \\ t_{1,1} p_1 & t_{2,2} p_2 & t_{3,3} p_3 & t_{4,1} & t_{5,2} & t_{6,3} \end{bmatrix}$$

$$[T_{t1} = \begin{bmatrix} \alpha_1 & \alpha_2 & \alpha_3 \\ 1 & 1 & 1 \\ \beta_1 & \beta_2 & \beta_3 \end{bmatrix}$$

$$[T_{t2}] = \begin{bmatrix} r_{1,1} & r_{2,2} & r_{3,3} \\ s_{1,1} & s_{2,2} & s_{3,3} \\ t_{1,1} & t_{2,2} & t_{3,3} \end{bmatrix}$$

$$[cT_1] = \begin{bmatrix} \alpha_1 & \alpha_2 & \alpha_3 & \alpha_4 q_1 & \alpha_5 q_2 & \alpha_6 q_3 & 0 & 0 & 0 & 0 & 0 & 0 \\ 1 & 1 & 1 & q_1 & q_2 & q_3 & 0 & 0 & 0 & 0 & 0 & 0 \\ \beta_1 & \beta_2 & \beta_3 & \beta_4 q_1 & \beta_5 q_2 & \beta_6 q_3 & 0 & 0 & 0 & 0 & 0 & 0 \\ 0 & 0 & 0 & 0 & 0 & 0 & \alpha_1 p_1 & \alpha_2 p_2 & \alpha_3 p_3 & \alpha_4 & \alpha_5 & \alpha_6 \\ 0 & 0 & 0 & 0 & 0 & 0 & p_1 & p_1 & p_1 & 1 & 1 & 1 \\ 0 & 0 & 0 & 0 & 0 & 0 & \beta_1 p_1 & \beta_2 p_2 & \beta_3 p_3 & \beta_4 & \beta_5 & \beta_6 \\ f_{1,1} q_1 & f_{2,2} q_2 & f_{3,3} q_3 & g_{4,1} & g_{5,2} & g_{6,3} & \alpha_1 q_1 & \alpha_2 q_2 & \alpha_3 q_3 & \alpha_4 o_1 & \alpha_5 o_2 & \alpha_6 o_3 \\ -r_{1,1} q_1 & -r_{2,2} q_2 & -r_{3,3} q_1 & r_{4,1} & r_{5,2} & r_{6,3} & r_{1,1} q_1 & r_{2,2} q_2 & r_{3,3} q_3 & r_{4,1} o_1 & r_{5,2} o_2 & r_{6,3} o_3 \\ h_{1,1} q_1 & h_{2,2} q_2 & h_{3,3} q_3 & j_{4,1} & j_{5,2} & j_{6,3} & q_1 & q_2 & q_3 & o_1 & o_2 & o_3 \\ -s_{1,1} q_1 & -s_{2,2} q_2 & -s_{3,3} q_3 & s_{4,1} & s_{5,2} & s_{6,3} & s_{1,1} q_1 & s_{2,2} q_2 & s_{3,3} q_3 & s_{4,1} o_1 & s_{5,2} o_2 & s_{6,3} q_3 \\ u_{1,1} q_1 & u_{2,2} q_2 & u_{3,3} q_3 & v_{4,1} & v_{5,2} & v_{6,3} & \beta_1 q_1 & \beta_2 q_2 & \beta_3 q_3 & \beta_4 o_1 & \beta_5 o_2 & \beta_6 o_3 \\ -t_{1,1} q_1 & -t_{2,2} q_2 & -t_{3,3} q_3 & t_{4,1} & t_{5,2} & t_{6,3} & t_{1,1} q_1 & t_{2,2} q_2 & t_{3,3} q_3 & t_{4,1} o_1 & t_{5,2} o_2 & t_{6,3} o_3 \end{bmatrix}$$

$$[cT_2] = \begin{bmatrix} r_{1,1} & r_{2,2} & r_{3,3} & r_{4,1} q_1 & r_{5,2} q_2 & r_{6,3} q_3 & 0 & 0 & 0 & 0 & 0 & 0 \\ s_{1,1} & s_{2,2} & s_{3,3} & s_{4,1} q_1 & s_{5,2} q_2 & s_{6,3} q_3 & 0 & 0 & 0 & 0 & 0 & 0 \\ t_{1,1} & t_{2,2} & t_{3,3} & t_{4,1} q_1 & t_{5,2} q_2 & t_{6,3} q_3 & 0 & 0 & 0 & 0 & 0 & 0 \\ 0 & 0 & 0 & 0 & 0 & 0 & r_{1,1} p_1 & r_{2,2} p_2 & r_{3,3} p_3 & r_{4,1} & r_{5,2} & r_{6,3} \\ 0 & 0 & 0 & 0 & 0 & 0 & s_{1,1} p_1 & s_{2,2} p_2 & s_{3,3} p_2 & s_{4,1} & s_{5,2} & s_{6,3} \\ 0 & 0 & 0 & 0 & 0 & 0 & t_{1,1} p_1 & t_{2,2} p_2 & t_{3,3} p_3 & t_{4,1} & t_{5,2} & t_{6,3} \end{bmatrix}.$$

Funding There is funding to report for this submission.

Data availability No data was used in this research.

Declarations

Conflict of Interest The author(s) declared no potential conflicts of interest with respect to the research, authorship, and/or publication of this article.

References

1. Farrar CR, Worden K (2007) An introduction to structural health monitoring. Phil Trans R Soc A 365(1851):303–315
2. Ostachowicz WM (2008) Damage detection of structures using spectral finite element method. Comput Struct 86(3–5):454–462
3. Grabowska J, Palacz M, Krawczuk M (2008) Damage identification by wavelet analysis. Mech Syst Signal Process 22(7):1623–1635
4. Rucka M (2010) Experimental and numerical studies of guided wave damage detection in bars with structural discontinuities. Arch Appl Mech 80(12):1371–1390
5. Rucka M (2010) Experimental and numerical study on damage detection in an L-joint using guided wave propagation. J Sound Vib 329(10):1760–1779
6. Saravanan TJ, Gopalakrishnan N, Rao NP (2015) Damage detection in structural element through propagating waves using radially weighted and factored RMS. Measurement 73:520–538
7. Doyle, J.F. (1989). *Wave Propagation in Structures. In: Wave Propagation in Structures*. Springer, New York.
8. Gopalakrishnan S, Martin M, Doyle JF (1992) A matrix methodology for spectral analysis of wave propagation in multiple connected Timoshenko beams. J Sound Vib 158(1):11–24
9. Gopalakrishnan S, Doyle JF (1994) Wave propagation in connected waveguides of varying cross-sections. J Sound Vib 175(3):347–363
10. He S, Ng CT, Yeung C (2020) Time-domain spectral finite element method for modeling second harmonic generation of guided waves induced by material, geometric and contact nonlinearities in beams. Int J Struct Stab Dyn 20(10):2042005
11. Yu H, Chen X, Li P (2022) Analytical solution for vibrations of a modified timoshenko beam on visco-pasternak foundation under arbitrary excitations. Int J Struct Stab Dyn 22(07):2250045
12. Modak, K., Saravanan, T. J., & Rajasekharan, S. (2023). Structural Damage Identification Using Spectral Finite Element Modeling for Extended Timoshenko Beams. In *Experimental Vibration Analysis for Civil Engineering Structures* (pp. 439–451). Springer, Cham.
13. Pind F, Engsig-Karup AP, Jeong CH, Hesthaven JS, Mejling MS, Strømann-Andersen J (2019) Time domain room acoustic simulations using the spectral element method. J Acoust Soc Am 145(6):3299–3310
14. Wu Z, Li F, Zhang C (2018) Band-gap analysis of a novel lattice with a hierarchical periodicity using the spectral element method. J Sound Vib 421:246–260
15. Wu ZJ, Li FM (2015) Dynamic properties of three-dimensional piezoelectric Kagome grids. Waves Random Compl Media 25(3):361–381
16. Wu ZJ, Li FM, Wang YZ (2013) Vibration band gap behaviors of sandwich panels with corrugated cores. Comput Struct 129:30–39
17. Wu ZJ, Li FM, Zhang C (2015) Vibration band-gap properties of three-dimensional Kagome lattices using the spectral element method. J Sound Vib 341:162–173

18. Mukherjee A, Sarkar S, Banerjee A (2021) Nonlinear eigenvalue analysis for spectral element method. Comput Struct 242:106367
19. Loya JA, Rubio L, Fernández-Sáez J (2006) Natural frequencies for bending vibrations of Timoshenko cracked beams. J Sound Vib 290(3–5):640–653
20. Aydin K (2007) Vibratory characteristics of axially-loaded Timoshenko beams with arbitrary number of cracks. J Vib Acoust 129(3):341–354
21. Aydin K (2008) Vibratory characteristics of Euler-Bernoulli beams with an arbitrary number of cracks subjected to axial load. J Vib Control 14(4):485–510
22. Masoud AA, Al-Said S (2009) A new algorithm for crack localization in a rotating Timoshenko beam. J Vib Control 15(10):1541–1561
23. Shi D, Wang Q, Shi X, Pang F (2015) An accurate solution method for the vibration analysis of Timoshenko beams with general elastic supports. Proc Inst Mech Eng C J Mech Eng Sci 229(13):2327–2340
24. Lee U (2000) Vibration analysis of one-dimensional structures using the spectral transfer matrix method. Eng Struct 22(6):681–690
25. Hu N, Fukunaga H, Kameyama M, Mahapatra DR, Gopalakrishnan S (2007) Analysis of wave propagation in beams with transverse and lateral cracks using a weakly formulated spectral method. J Appl Mech 74(1):119–127
26. Chakraborty A, Gopalakrishnan S (2003) A spectrally formulated finite element for wave propagation analysis in functionally graded beams. Int J Solids Struct 40(10):2421–2448
27. Krawczuk M, Palacz M, Ostachowicz W (2004) Wave propagation in plate structures for crack detection. Finite Elem Anal Des 40(9–10):991–1004
28. Żak A (2009) A novel formulation of a spectral plate element for wave propagation in isotropic structures. Finite Elem Anal Des 45(10):650–658
29. Zhu X, Li TY, Zhao Y, Liu JX (2006) Structural power flow analysis of Timoshenko beam with an open crack. J Sound Vib 297(1–2):215–226
30. Kudela P, Żak A, Krawczuk M, Ostachowicz W (2007) Modelling of wave propagation in composite plates using the time domain spectral element method. J Sound Vib 302(4–5):728–745
31. Peng H, Meng G, Li F (2009) Modeling of wave propagation in plate structures using three-dimensional spectral element method for damage detection. J Sound Vib 320(4–5):942–954
32. Saravanan TJ, Gopalakrishnan N, Rao NP (2017) Detection of damage through coupled axial–flexural wave interactions in a sagged rod using the spectral finite element method. J Vib Control 23(20):3345–3364
33. Kumar KV, Saravanan TJ, Sreekala R, Gopalakrishnan N, Mini KM (2017) Structural damage detection through longitudinal wave propagation using spectral finite element method. Geomech Eng 12(1):161–183
34. Saravanan TJ, Gopalakrishnan N, Rao NP (2018) Experiments on coupled axial–flexural wave propagation in a sagged rod with structural discontinuity using piezoelectric transducers. J Vib Control 24(13):2717–2731
35. Sarvestan V, Mirdamadi HR, Ghayour M (2017) Vibration analysis of cracked Timoshenko beam under moving load with constant velocity and acceleration by spectral finite element method. Int J Mech Sci 122:318–330
36. Ni Z, Hua H (2018) Axial-bending coupled vibration analysis of an axially-loaded stepped multi-layered beam with arbitrary boundary conditions. Int J Mech Sci 138:187–198
37. Naderi A, Behdad S, Fakher M, Hosseini-Hashemi S (2020) Vibration analysis of mass nanosensors with considering the axial-flexural coupling based on the two-phase local/nonlocal elasticity. Mech Syst Signal Process 145:106931
38. Banerjee JR, Ananthapuvirajah A (2019) Coupled axial-bending dynamic stiffness matrix for beam elements. Comput Struct 215:1–9
39. Banerjee JR, Ananthapuvirajah A, Liu X, Sun C (2021) Coupled axial-bending dynamic stiffness matrix and its applications for a Timoshenko beam with mass and elastic axes eccentricity. Thin-Wal Struct 159:107197
40. Lee U, Lee C (2009) Spectral element modeling for extended Timoshenko beams. J Sound Vib 319(3–5):993–1002
41. Palacz M, Krawczuk M (2002) Analysis of longitudinal wave propagation in a cracked rod by the spectral element method. Comput Struct 80(24):1809–1816
42. Krawczuk M, Palacz M, Ostachowicz W (2003) The dynamic analysis of a cracked Timoshenko beam by the spectral element method. J Sound Vib 264(5):1139–1153
43. Tada, H., Paris P.C., & Irwin, G.R. (2000) *The Stress Analysis of Cracks Handbook*, Third Edition, *ASME Press.*
44. Cowper GR (1966) The shear coefficient in Timoshenko's beam theory. J Appl Mech 33(2):335–340
45. M. Krawczuk, 1994 Dynamics of Constructional Elements with Fatigue Cracks, 441, IFFM Publishers, gdansk, , p. 1398